Journal of Polymers and the Environment (2023) 31:2032–2054
https://doi.org/10.1007/s10924-022-02705-w

ORIGINAL PAPER

Effective Bio-Sorbents for the Simultaneous Removal of Cadmium and Mercury Ions from Polluted Waters: Based on *Ficus Panda* Plant Areal Roots Active Carbon, Nano Particle of SnO_2 and Al-Alginate Beads

Miriyala Sudhakar[1] · Vallela Siva Reddy[1] · Suneetha Mekala[2] · Kunta Ravindhranath[1]

Accepted: 21 November 2022 / Published online: 19 December 2022

Abstract
In the present investigation *Ficus Panda* areal roots powder (FPARP) and its active carbon (FPARAC) are identified to adsorb Cd^{2+} and Hg^{2+}. The adsorptivities are increased further when the active carbon is doped with green synthesized $nSnO_2$ (FPARAC.$nSnO_2$). To prevent 'agglomeration' of nanoparticles and make filtration easy, the composite of active carbon and $nSnO_2$ are embedded in Al-alginate beads (FPARAC.$nSnO_2$-Al.alg). The beads have shown cumulative sorption nature and the sorption capacities are as high as: 12.8 mg/g for Cd^{2+} and 10.0 mg/g for Hg^{2+}. The $nSnO_2$ particles are synthesized by new green methods adopting *aloe-vera* gel as capping agent. The extraction conditions are optimized and noted that simultaneous removal of Cd^{2+} and Hg^{2+} is possible at pH: 5 with FPARP and pH: 6 with rest of the adsorbents. The adsorbents are characterized by employing XRD, FTIR and FESEM techniques. The thermodynamic studies have shown that the adsorption process is 'spontaneous' and 'endothermic' in nature with all sorbents. The high values of ΔH° suggest that the mechanism of adsorption is via surface complex formation and is well supported by FTIR investigations. The spent adsorbents are regenerated by treatment with 0.1 N HCl and can be reused. These adsorbents are successfully applied to treat real wastewater samples of industries contaminated with Cd^{2+} and Hg^{2+} ions. The novelty of the present investigation is that highly efficient adsorbents are developed for the simultaneous removal of highly toxic Cd^{2+} and Hg^{2+} ions from polluted water by evoking the cumulative sorption nature of $nSnO_2$, *Ficus Panda* areal roots active carbon and Al-alginate beads.

✉ Kunta Ravindhranath
ravindhranath.kunta@gmail.com

[1] Department of Chemistry, Koneru Lakshmaiah Education Foundation, Green Fields, Vaddeswaram, Guntur, Andhra Pradesh 522 502, India

[2] Department of Chemistry, RGUKT-Nuzvid, Nuzvid, Andhra Pradesh, India

Graphical Abstract

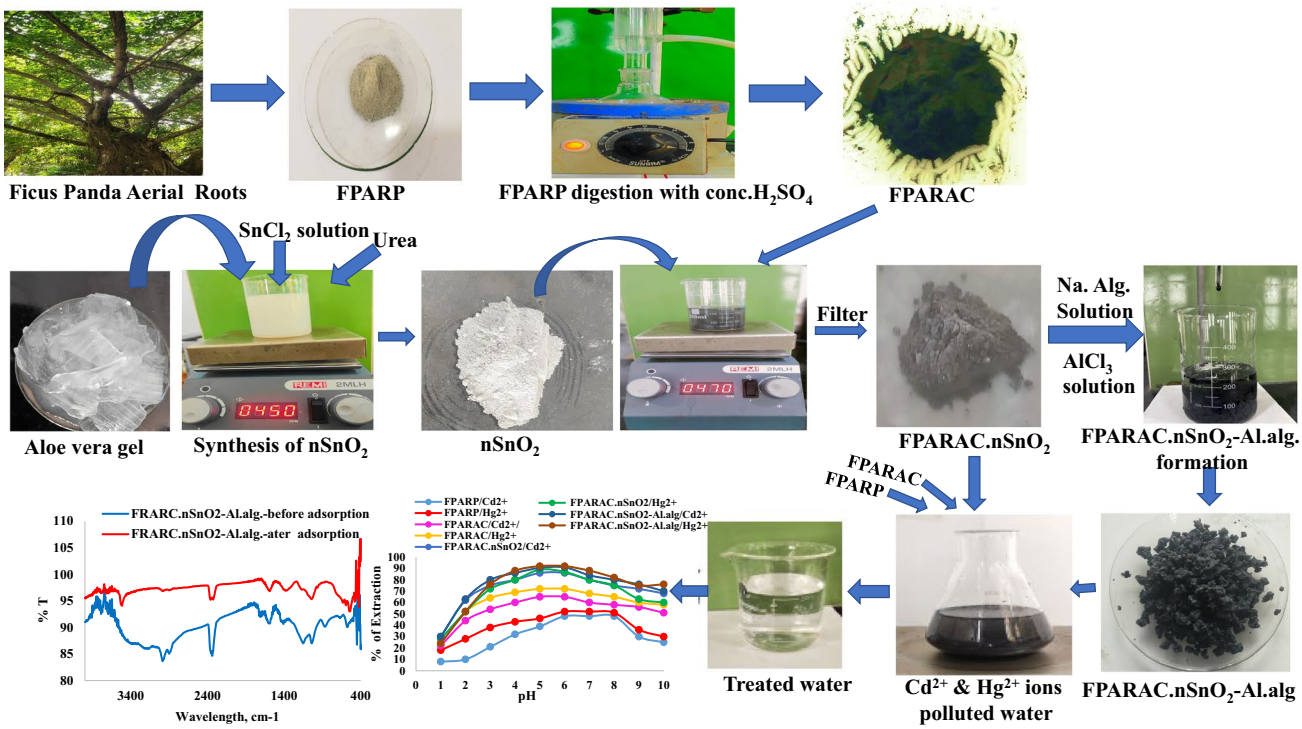

Keywords *Ficus Panda* plant · *Aloe-vera* gel · Nano SnO_2 · Batch adsorption · Cadmium and mercury ions · Applications

Introduction

The pollution of waterbodies with toxic ions is increasing felt with the progress of industrialization, urbanization, and development of human civilization. The large quantities of untreated wastewater released especially from various industries into natural water bodies, is endangering the human sustainability. Of the major pollutants, heavy metal ions especially cadmium and mercury ions are highly toxic even at low concentrations [1]. The maximum permissible concentrations as per WHO are: 0.003 mg/L for Cd^{2+} and 0.001 mg/L for Hg^{2+} ions [2]. They cause serious threat to the aquatics, humans, and vegetation to a great extent [3]. These ions are accumulated in food chains and cause severe diseases such as '*itai-itai*' due to cadmium toxicity in humans and '*minamata*' disease due to mercury poisoning [4, 5]. Other ailments caused by these toxic ions are cancer, damaging of CNS system, skin dermatitis, brain, liver, heart, lungs, kidney dysfunction, retardation of growth and even death [1, 3–6].

Cadmium and mercury ions enter water bodies through two main sources: natural and anthropogenic activities. Natural sources are volcanic eruptions, weathering of rocks and minerals and soil erosion. Anthropogenic sources include mining operations, petroleum refining, nickel–cadmium batteries, coal combustion, electroplating, alloying industry, dental filling, amalgamation, tanneries, plastic stabilizers, solders, rectifiers, catalysts, agricultural activities, Hg vapor lamps, pharmaceuticals, fungicides etc. [2]. Hence, there is dire necessity to treat cadmium and mercury contaminated wastewater before discharging it into water bodies.

The water remediation methods for Cd^{2+} and Hg^{2+} ions, have been investigated based on the conventional methods such as chemical precipitation, coagulation/flocculation, solvent extraction, ion-exchange, oxidation, membrane separation, electro dialysis, ultrafiltration etc. [7, 8]. However, these methods suffer from one or other dis-advantages such as: expensive, hazardous by-products formation, low efficiencies, difficulty in regeneration and incomplete metal removal [9]. In this context, the adsorption methods especially based on employing bio-materials as adsorbents is promising and generating the global interest because the methods are simple, effective and economical [5, 10]. The bio-computability of the bio-materials and their renewable sources are the inherent merits of this aspect of water remediation methods [10–12].

Various adsorbents such as marine macro alga, activated carbon, goethite, multi walled carbon nanotubes,

sugar cane bagasse, poly(m-phenylene diamine) microparticles, peanut shells, saw dust bentonite, hydroxyapatite, waste tea leaves, two dimensional metal carbides, silica, hydroxyl apatite, rice husk, magnetic nanoparticles, nano-silica soybean hulls, magnetic nano-adsorbent, nano-alumina, urea-grafted alginate, Moringa species, Alginate and Chitosan modifications etc. have been investigated for the removal of cadmium or mercury ions [1, 4–6, 8, 13–15]. Most of these methods are used to remove either mercury or cadmium ions separately but not both the ions simultaneously.

The major disadvantage of these bio-adsorbents is that they suffer from low adsorptivities. But incorporating nano materials in the matrix of bio-materials the adsorption capacity of the resultant mixed adsorbent may be enhanced in some instances because of unique characteristics of nano materials such as small particle size, large surface area, large pore volume, high adsorption capacity and fast rate of adsorption [5]. Though biomaterial (active carbon) structure prevents 'agglomeration' of nano particles to some extent, it cannot be avoided completely. Hence, investigations are being undertaken to incorporate the composite of 'nano particles and active carbon' in beads. As alginate beads and plant-based materials are non-toxic, biodegradable, biocompatible, more abundant and inexpensive, they are increasing used in wastewater treatment [10, 14]. The present work is an attempt in this direction.

Further, the nanoparticles synthesized from conventional physical and chemical methods are not eco-friendly because of the use of toxic reducing and stabilizing synthetic reagents. Adoption of plant extracts as substitutes for capping agents in the synthesis of nano particle is another recent advance. In this investigation, we identified biomaterials of *Ficus Panda* areal roots have the adsorptivity for both Cd^{2+} and Hg^{2+} ions. The sorption nature is increased further when the active carbon of the said plant material is doped with green synthesized nano SnO_2. In this investigation, *Aloe-vera* gel extract is identified as capping agent for the synthesis of SnO_2 nanoparticles of size: 31.3 nm. To prevent agglomeration of nanoparticles and make filtration easy, the composite of 'active carbon and $nSnO_2$' is doped in Al-alginate beads (FPARAC.$nSnO_2$-Al.alg). The beads have shown high adsorptivity due to the cumulative sorption nature of active carbon, $nSnO_2$ and Al-alginate beads for the simultaneous removal of Cd^{2+} and Hg^{2+} ions. This is the novelty of the present work. Thus, the present article is a comprehensive narration of synthesis of adsorbents, their characterization, and their adoptability as adsorbents for the simultaneous removal of Cd^{2+} and Hg^{2+} ions from polluted water.

Experimental

Materials

Chemicals and Solutions

A.R. grade chemicals and reagents were used throughout in this research work. All the chemicals were purchased from Merck. India Pvt. Ltd. and S.D. Chemicals, India. The required solutions were prepared as described in the literature [16]. The simulated stock solutions of cadmium (20.0 mg/L) and mercury (15.0 mg/L) were prepared using distilled water.

Preparation of Adsorbents

Ficus Panda Aerial Roots Powder

Ficus Panda aerial roots were cut from the plant, washed with distilled water and dried at 105 °C for 1.0 h in a hot air oven and crushed to powder. The powder was meshed through 75 size. It was named as FPARP.

Ficus Panda Aerial Roots Active Carbon

Required quantity of raw *Ficus Panda* aerial roots powder was taken into a round bottom flask of required size and needed quantity of conc. H_2SO_4 was added and kept it a side for over-night for digestion. Then the flask along with material was connected to a water condenser and subjected to heating under conductive distillation until all the material was completely charred. Then the contents in the flask were diluted with distilled water and filtered for the bio-char. Thus produced bio-char was washed with distilled water for neutrality, oven-dried at 110 °C for one hour and stored in a brown bottle. It was named as FPARAC.

Ficus Panda Aerial Roots Active Carbon Loaded with $nSnO_2$

Synthesis of Nano-SnO_2 via New Green Routes In the present investigation new green methods were investigated by replacing toxic synthetic capping agents by eco-friendly plant extracts and by evoking homogeneous methods of generating the precipitating agent in a viscous media composed of water: ethylene glycol (80:20). The approach was adopted with a view that slow generation of precipitating agent in highly viscous medium coupled with the 'capping and stabilizing abilities' of naturally existing compounds in the plant extracts will prevent the growth of the particles beyond nano size. We tried various plant extracts and noticed that *Aloe-vera* gel has capping ability in controlling the size of the

particles. Further, the precipitating agent was generated by Urea hydrolysis in the viscous medium composed of ethylene glycol and water (20:80). Thus, we were successful in 'tailor-making' the size of SnO_2 to nano size.

The Aloe-Vera Gel Extract The gel was scrapped from the folded leaves of the plant. 50 g of the gel was taken into a 250 mL round bottom flask and to it, 100 mL of distilled water was added and connected to a water condenser. Then the contents in the flask were heated for one hour under water-condenser set up, collected and filtered. The filtrate was collected and preserved in refrigerator at 5.0 °C.

Synthesis of $nSnO_2$ 5.0 g of A.R. $SnCl_2$ was taken in a 250 mL beaker. 150 mL of water: glycerol (80:20) and 1.0 mL of conc. HCl were added and mixed well using magnetic stirrer. When all the salt was dissolved, 25.0 mL of *aloe-vera* gel and 5.0 g of Urea were added. While continuing the stirring, the contents in the beaker were slowly heated until the temperature reached to 80 °C. As the temperature was gradually increased, ammonia was liberated increasingly due to the hydrolysis of Urea and as a result, pH of the solution was increased. When the solution attained pH: 9, the heating was stopped but stirring was continued for 2.0 more hrs at 550 rpm. Thus obtained material was centrifuged, washed with distilled water for neutrality and oven-dried at 110 °C. The material was then calcinated at 500 °C for 4 h in Muffle furnace. Thus obtained material was characterized.

Synthesis of FPARAC.$nSnO_2$ 5.0 g of FPARAC was taken in 100 mL of distilled water and stirred at 500 rpm using magnetic stirrer and while stirring 2.0 g of $nSnO_2$was added and continued the stirring for 1.0 h. Then the material was set aside for over-night, filtered and dried at 110 °C for 2.0 h. Thus $nSnO_2$ admixed or loaded FPARAC was termed as: FPARAC.$nSnO_2$.

Synthesis of Al-Alginate Beads Embedded with FPARAC.$nSnO_2$ 2.5% (w/v) Sodium alginate in water was subjected to magnetic-stirring at 500 rpm while heating slowly to reach a temperature of 70 °C, resulting a 'gel-like' solution. Then 5.0 g of 'FPARAC.$nSnO_2$' was added and continued the stirring for one hour to homogenize the solution. Then the solution was cooled to room temperature and added in drop wise to the cooled 3.0% acidic $AlCl_3$ solution (10 °C). The moment the drops touches the solution, beads were formed due to the cross-linking of Na-alginate with Al^{3+} ions and in that formation, the 'FPARAC.$nSnO_2$' was trapped or embedded. Thus formed beads, FPARAC.$nSnO_2$-Al.alg, were allowed to be digested for over-night with the mother liquor for attaining the uniform size. Beads were filtered and thoroughly washed for neutrality with distilled-water. Then the beads were dried at 75 °C for 1.0 h in hot-air oven. The various stages of preparation of these four adsorbents were presented graphically in the Fig. 1.

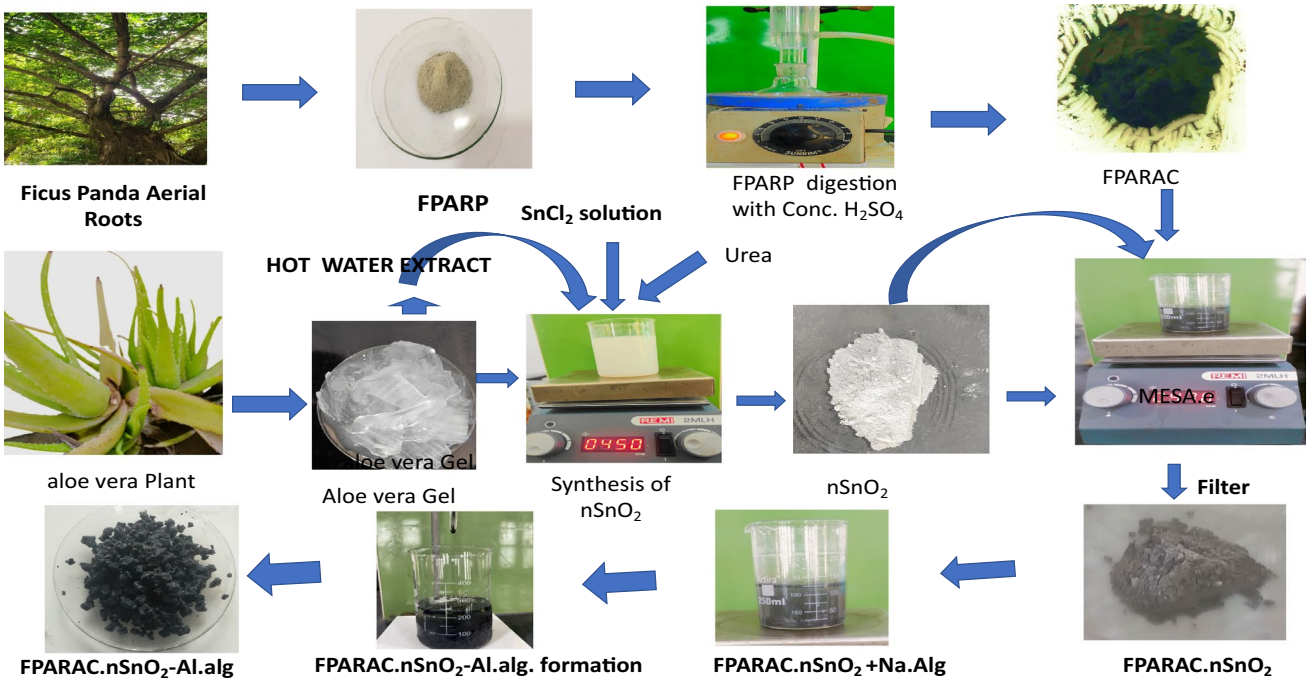

Fig. 1 Various stages of synthesis of adsorbents

Characterization and Methods

Characterization

The developed adsorbents in this study were characterized for different physicochemical parameters such as moisture (%) [17], apparent density (g/mL) [17], Iodine number (mg/g) [18], ash (%) [19], particle size (μ) [20] and BET-surface area (m^2/g) [21] as per standard procedures in the literature. The results were presented in the Table 1.

X-ray diffraction (XRD) and Fourier Transform Infrared (FTIR) spectroscopy and Field Emission and Scanning Electron Microscopic (FESEM) were adopted to know the surface characteristics of the adsorbents, 'before and after' adsorption of cadmium and mercury ions.

PAN analytical X-ray diffract meter using Cu Kα source at 1.54 A^o was used to measure the XRD patterns of the adsorbents. FTIR spectra was noted by BRUKER ALFA FTIR spectrophotometer (KBr pellet method) in the range 4000–500 cm^{-1}. FESEM images were noted using the instrument FESEM, Zeiss, Sigma, Germany equipped with FESEMEDX at the optimum voltage of 3.0 kV with ultra-high resolution. The results obtained were presented in Figs. 2, 3, 4 and 5.

Batch Mode Adsorption Experiments

In the present study, the adsorption performance of the developed adsorbents towards cadmium and mercury ions was assessed by adopting the batch mode of experiments. 100 mL of each Cd^{2+} (20.0 mg/L) and/or Hg^{2+} (15.0 mg/L) solutions were taken in stoppered flasks. Then, weighed quantities of adsorbents were added and pH of the solutions was adjusted in between 2 and 12 by using dil. HCl/dil. NaOH. Then, the flasks were agitated in an orbital-shaker at 350 rpm for a pre-determined period at a temperature of 30 ± 1 °C. After

Table 1 The evaluated physicochemical parameters

S. no.	Parameter	Value			
		FPARP	FPARAC	FPARAC.nSnO$_2$	FPARAC. nSnO$_2$-Al. alg
1	Moisture content (%)	8.54	7.23	6.14	5.36
2	Apparent density (g/mL)	0.291	0.327	0.483	0.572
3	Iodine number (mg/g)	605	513	428	391
4	Ash content (%)	4.57	3.14	2.98	2.31
5	Particle size (μ)	48.2	42.3	35.4	32.4
6	BET-surface area (m^2/g)				
	Before:	368.7	465.4	486.5	498.1
	After (Cd^{2+}):	314.2	291.3	273.6	247.9
	After (Hg^{2+}):	309.5	284.2	268.7	231.5

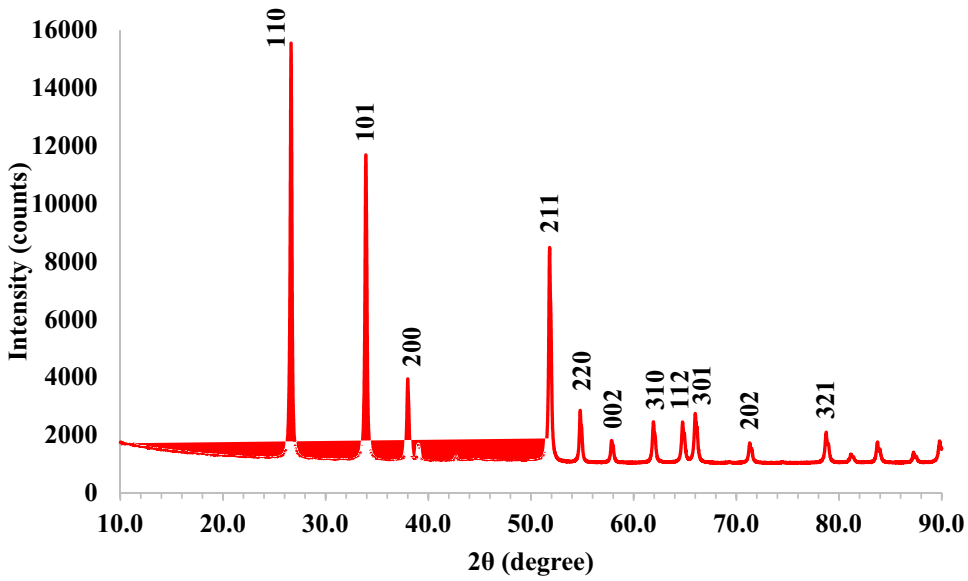

Fig. 2 XRD pattern of SnO_2

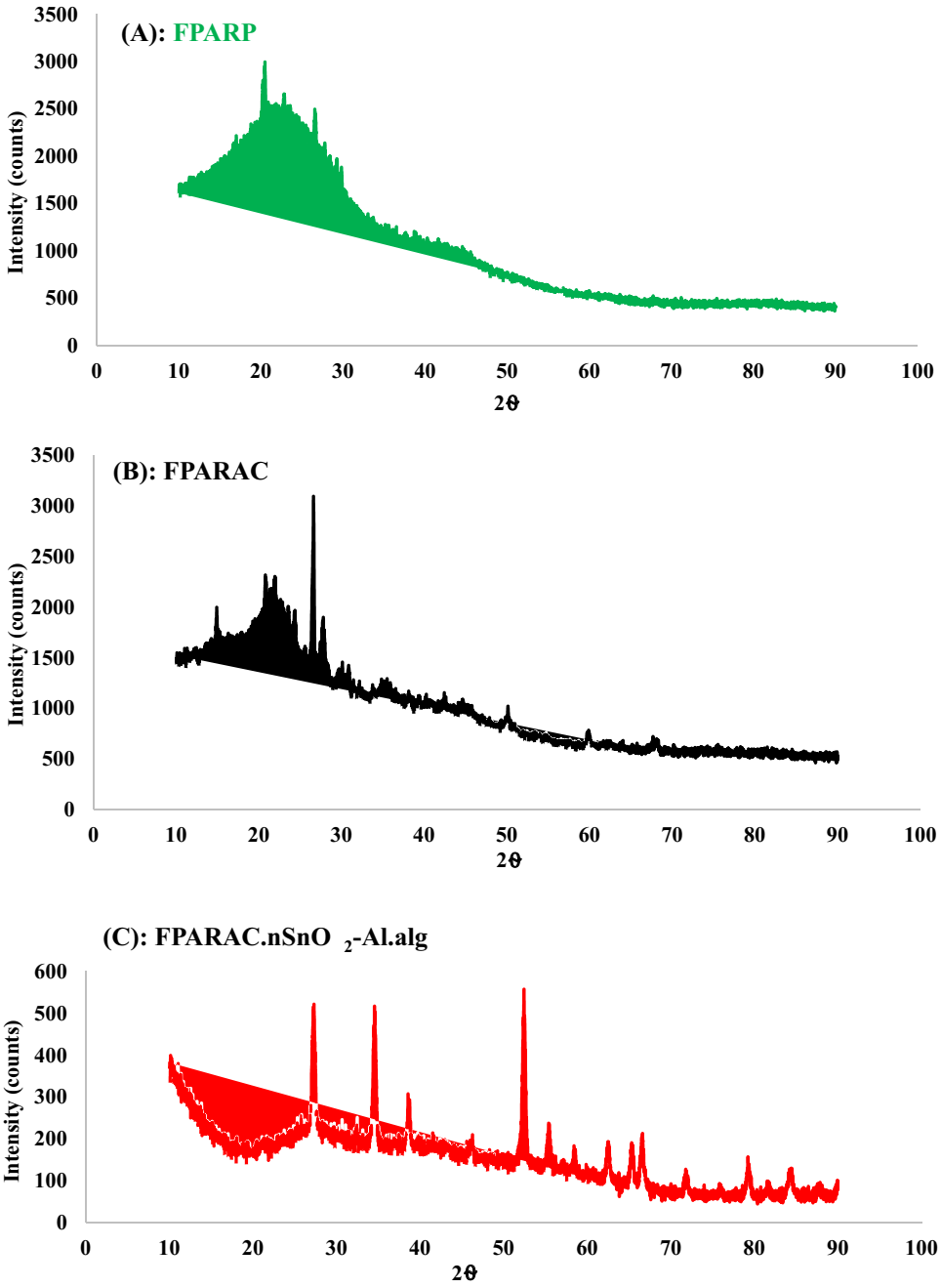

Fig. 3 XRD Spectrum of **A** FPARP, **B** FPARAC, **C** FPARAC.nSnO$_2$-Al.alg

reaching equilibration time, the solutions were filtered. The filtrates were analyzed for the concentrations of lead and mercury by adopting AAS method as described in elsewhere [22, 23]. Percentage removal and adsorption capacity were assessed by using the following equations.

$$\text{Adsorption capacity}: (q_e) = \frac{(C_i - C_e)}{m} V$$

$$\%\ \text{removal}\ (\%\ R) = \frac{(C_i - C_e)}{C_i} \times 100$$

where C_i = initial Cd^{2+}/Hg^{2+} concentration; Ce = equilibrium Cd^{2+}/Hg^{2+} concentration; and V = simulated solution volume (L); m = sorbent mass (g), were evaluated.

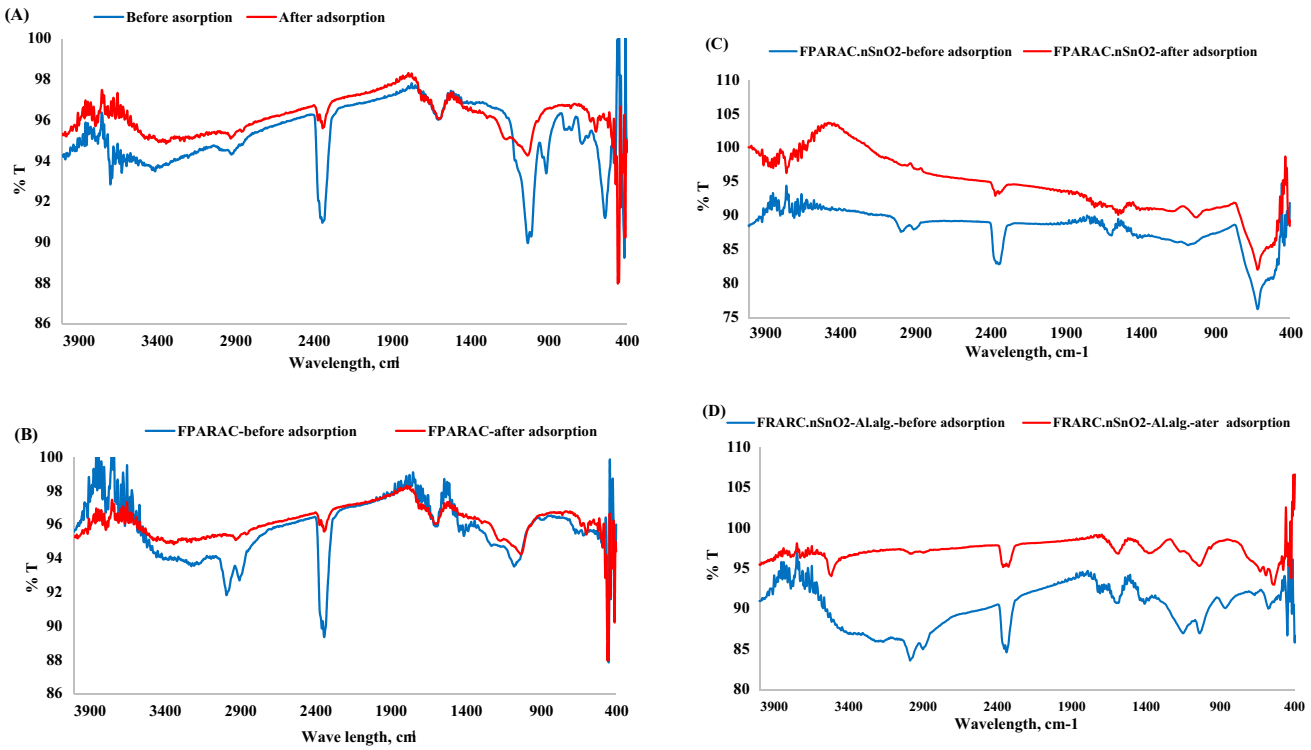

Fig. 4 **A** FTIR Spectra of FPARP-before and after adsorption of Cd^{2+} and Hg^{2+} ions. **B** FTIR Spectra of FPARAC-before and after adsorption of Cd^{2+} and Hg^{2+} ions. **C** FTIR Spectra of FPARAC.nSnO_2-before and after adsorption of Cd^{2+} and Hg^{2+} ions. **D** FTIR Spectra of FPARAC.nSnO_2-Al.alg-before and after adsorption of Cd^{2+} and Hg^{2+} ions

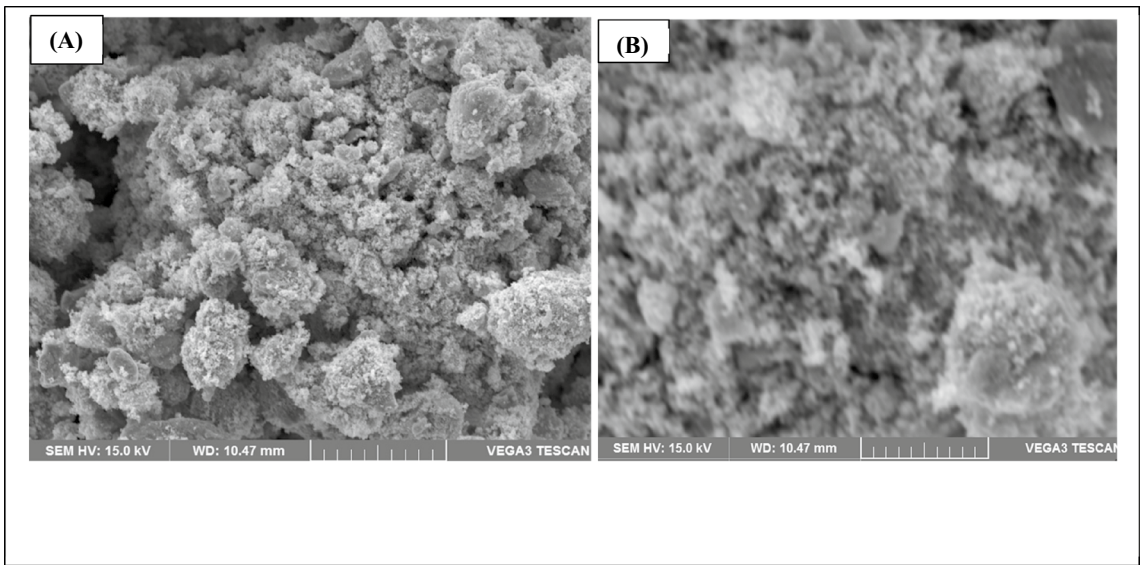

Fig. 5 FESEM images of FPARAC.nSnO_2-Al.alg: **A** before adsorption, **B** after adsorption of Cd^{2+} and Hg^{2+} ions

During these experiments, the optimum extraction conditions for the individual removal of cadmium and mercury were established by varying targeted parameter progressively and maintaining all other extraction conditions at constant values. Interference of co-ions on extraction and regeneration of spent adsorbents were

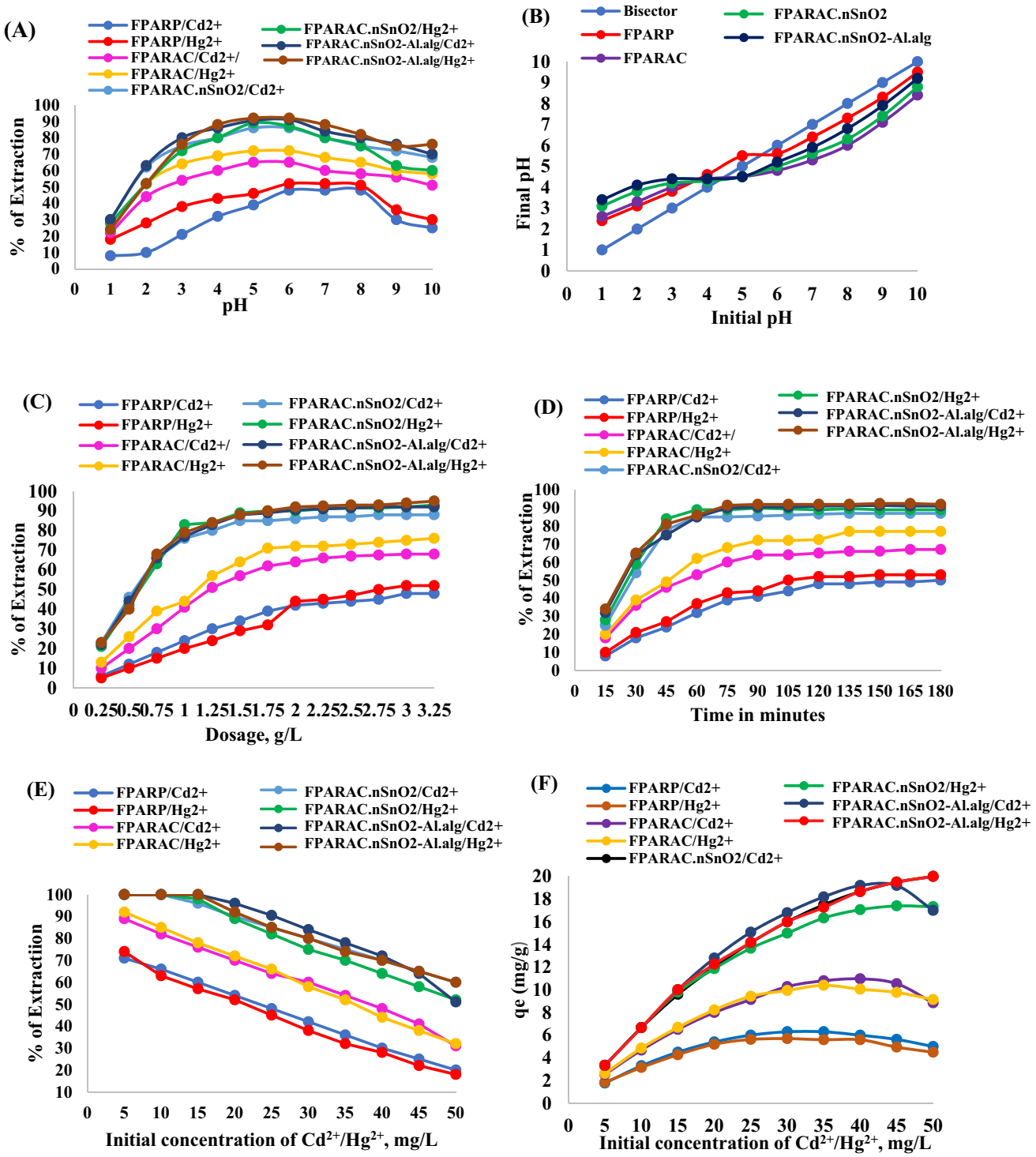

Fig. 6 Effect of: **A** pH; **B** pHzpc; **C** dosage; **D** time of equilibration; **E** initial concentration of Cd^{2+}/Hg^{2+}. **F** Sorption capacity vs initial concentration of Cd^{2+}/Hg^{2+}

also investigated. The mechanism of the adsorption process was analyzed by calculating adsorption isothermal, kinetic and thermos-dynamical parameters. The optimum extraction conditions for the simultaneous removal of cadmium and mercury were also investigated. The methodology developed in this study was used to treat real polluted

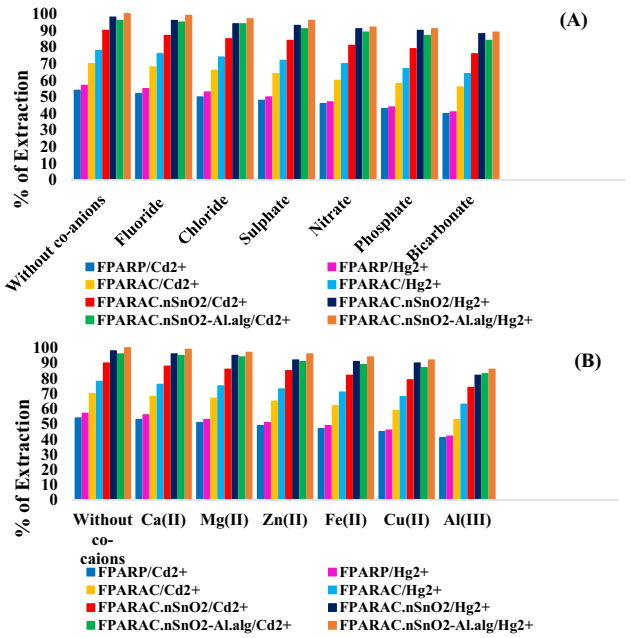

Fig. 7 Interference of co-ions: **A** Co-anions, **B** Co-cations

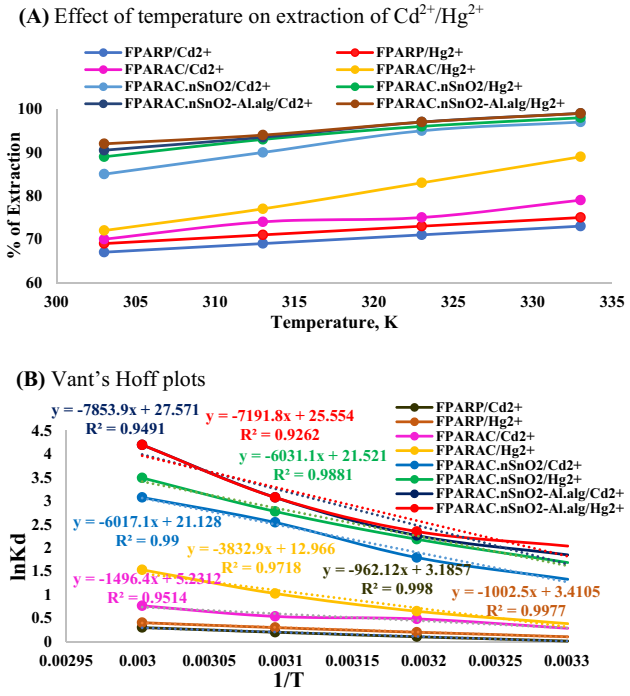

Fig. 8 **A** Effect of temperature on extraction of Cd^{2+}/Hg^{2+}. **B** Vant's Hoff plots

water samples. For all these experiments, the results were presented in Figs. 6, 7, 8, 9, 10 and 11 and Tables 1 and 7.

Results and Discussion

Characterization Studies

Physicochemical Parameters

As per the standard procedures described in elsewhere [11, 24, 25], the values of different physicochemical parameters of the adsorbents developed in this study were evaluated and presented in Table 1.

As it can be seen from the Table 1, the values of various physicochemical parameters confirmed that these biomaterials are good adsorbents. Further, the change in the BET-surface area values of the adsorbents 'before' and 'after' adsorption of cadmium and mercury ions also confirmed that these adsorbents have high adsorption capacities.

XRD Analysis

XRD spectra observed for $nSnO_2$, FPARP, FPARAC, FPARAC.$nSnO_2$-Al.alg were presented in Figs. 2 and 3A–C. The XRD pattern of $nSnO_2$ consists of a number of sharp peaks at 2θ values: 26.63°, 33.9°, 37.98°, 51.82°, 54.81°, 57.96°, 61.91°, 64.75°, 65.99°, 71.37° and 78.76°, which may arise due to diffractions at the planes: (110), (101), (200), (211), (220), (002),(310), (112), (301), (202) and (321) respectively. These patterns of peaks are as per JCPDS Card No: 41-1445, indicating rutile tetragonal crystalline phase of $nSnO_2$.

The crystallite size was evaluated (Table 2) adopting the Scherrer formula [26]:

$$L = \frac{k\lambda}{BCOS\theta}$$

where λ = radiation wavelength; B = physical width of a reflection (in 2θ); θ = diffraction angle of a line maximum; and K is a constant of value ≈0.9). The SnO_2 crystallite size was: 31.3 nm (average).

The XRD of 'FPARP' is characterized by a broad peak between 14.04° and 29.62° with an apex at 23.0°. Further on the hump of the broad peak some sharp shoots at 2θ values: 20.53°, 23.19°, 26.67° and 27.72° were noticed. The broadness of the peak is the characteristic of amorphous nature while the sharp shoots indicate some degree of crystallinity. The *Ficus Panda* aerial roots are subjected to aerial oxidation during their life time and hence, the roots powder is endowed with some degree of crystallinity besides dominant amorphous nature.

The XRD spectrum of FPARAC shows a characteristic broad peak of amorphous carbon between 18.9° and 25.8° with small off shoots at 20.91° and 21.97°. A sharp

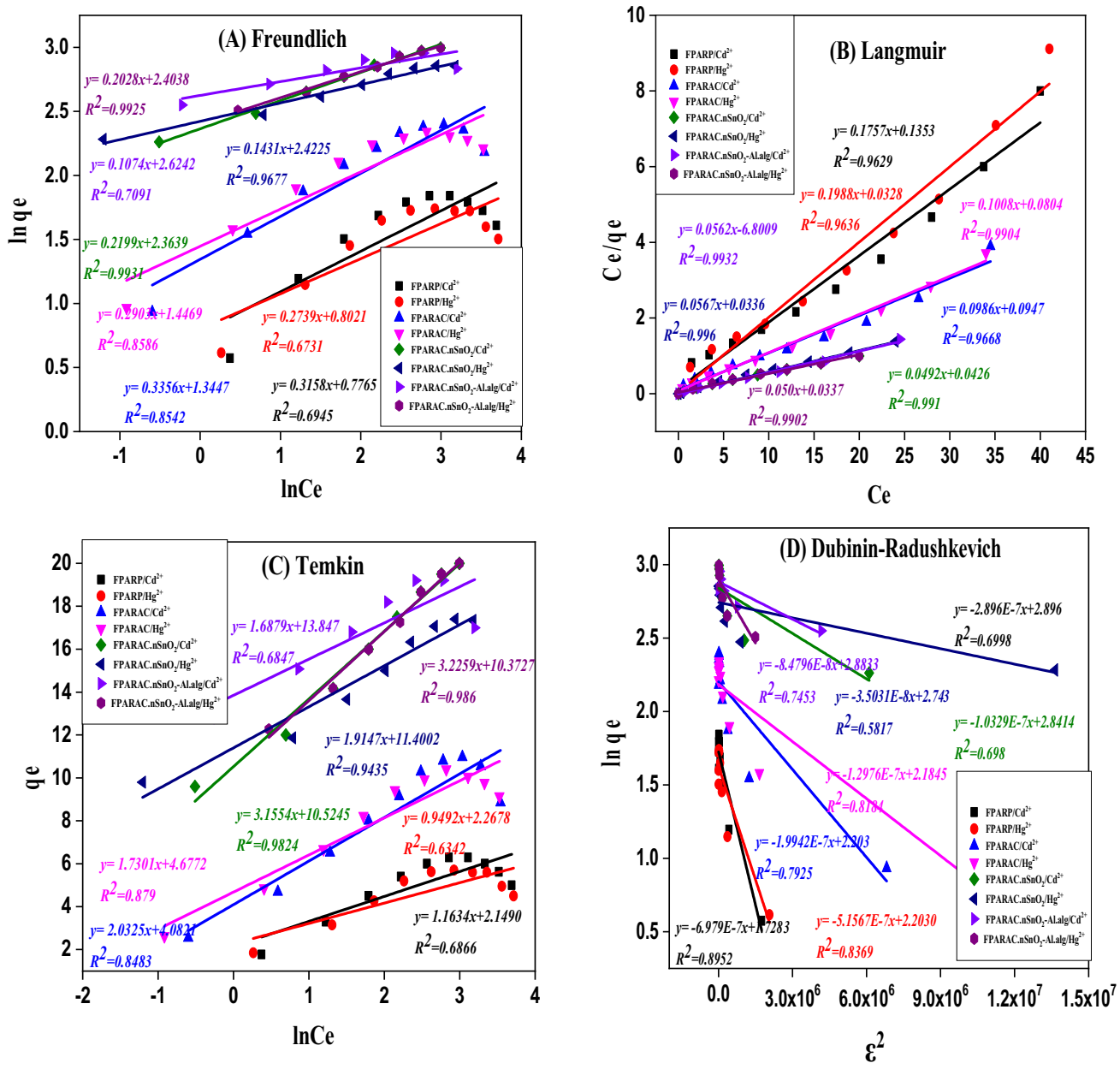

Fig. 9 Sorption Isotherm models: **A** Freundlich model; **B** Langmuir model; **C** Temkin model; **D** Dubinin–Radushkevich model

intensive peak at 26.55° and medium intensive peak at 27.98° are due to graphitic carbon [23]. The other sharp peaks with varying intensities at 15.13°, 50.96°, 60.08° and 68.37° are attributed to the crystallinity or order that prevails in the active carbon [27]. It may be inferred that a little degree of crystallinity acquired by the aerial roots is further increased in their active carbon.

The XRD spectrum of 'FPARC.SnO_2-Al.alg' is very interesting as the spectrum is endowed with sharp bands and broadness of band seen in the active carbons is almost vanished. The XRD pattern shows: prominent peaks with good intensities at: 27.34°, 34.59°, 52.59° and medium or small peaks of varying intensities at: 38.63°, 55.56°, 62.62°, 65.61°, 66.67°, 79.51° and 84.66°. On comparison of the XRD pattern of $nSnO_2$ with 'FPARAC.SnO_2-Al.alg', most of the peaks in the active carbon are altered or disappeared and some new peaks of $nSnO_2$ are noticed. The presence of many sharp peaks is an indicative of more crystallinity in the beads doped with $nSnO_2$ (FPARAC.SnO_2-Al.alg), than with active carbon (FPARAC) and roots powder (FPARP). In other words, the $nSnO_2$ and Al-alginate brought order in the carbon chains in active carbon either through bandings

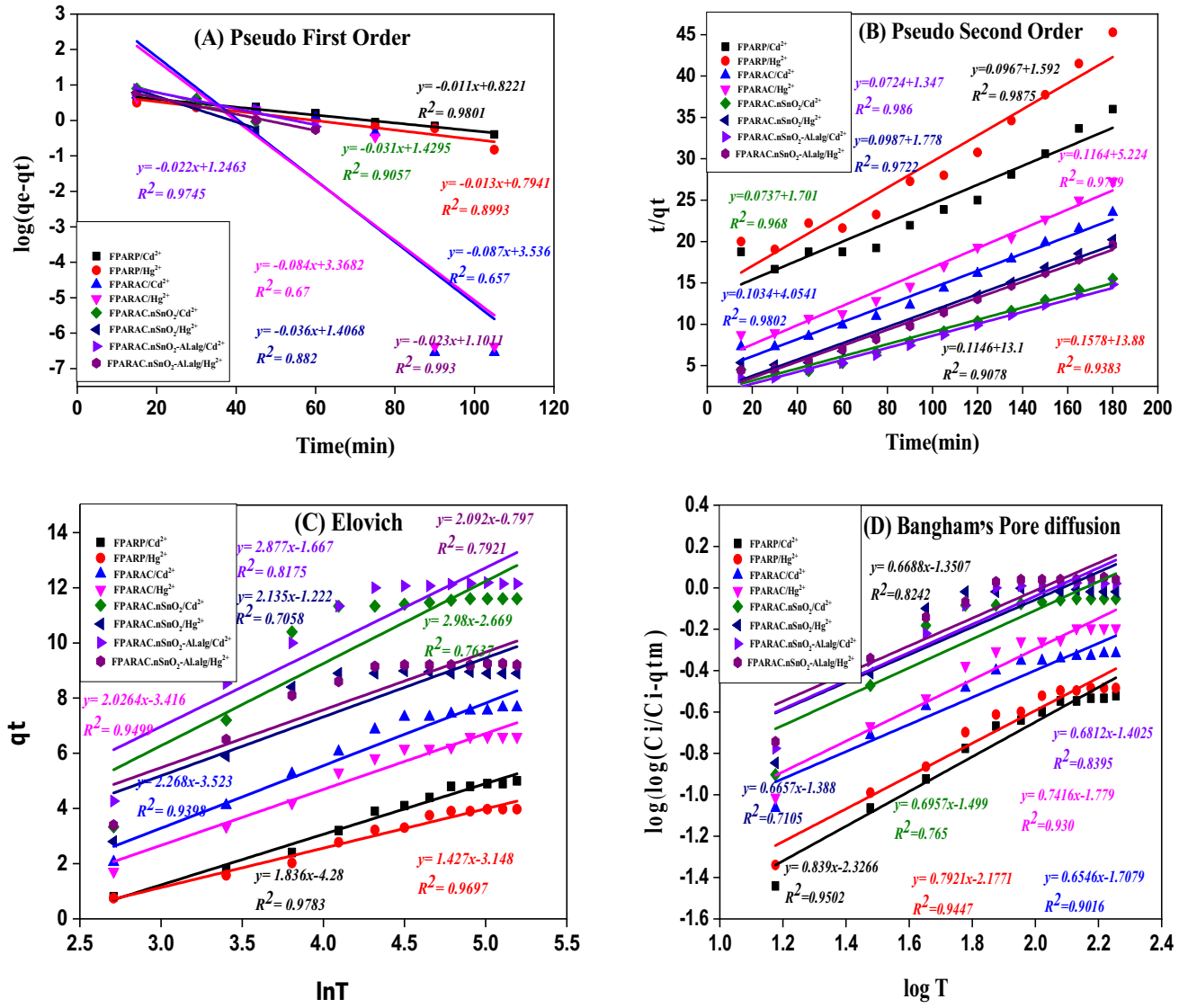

Fig. 10 Adsorption kinetics: **A** Pseudo 1st order kinetics; **B** Pseudo 2nd order kinetics; **C** Elovich model; **D** Bangam's pore diffusion models

or due to columbic interactions [27]. When the order is more in the matrix of the adsorbent, more facile is the movement of ions, which penetrate deeper from the adsorbent surface to reach the hidden adsorption sites. This manifests in good adsorptivity of the sorbent.

FTIR Analysis

Marked difference between the spectral features of the adsorbents taken 'before' and 'after' adsorption of Cd^{2+} and Hg^{2+} ions were observed. FTIR spectra showed the presence of various functional groups such as, –OH, –COOH,–NH, C=C, –C=O and > C–O on the surface of adsorbents [13]. In the case of 'FPARP', Fig. 4A, the broad bands generally appear in natural materials pertaining to intermolecular hydrogen bond among '–OH/–NH–' groups is absent. But sharp peaks of varying intensities appeared at: 3693, 3621, 3619 and 3515 cm^{-1}, indicating that the structures of *Ficus Panda* aerial roots are accomplished with free functional groups of –OH and –NH capable of bond formation with proper metal ions [28]. These spectral features are drastically reduced or disappeared and only a small peak at shifted frequency, 3788 cm^{-1} noted in the after-adsorption spectrum, indicating bond formation between functional –OH/–NH groups and metal ions [29].

The emphatic intensive peaks pertaining to 'conjugated system' at 2327 cm^{-1} and '–C–O' at 1029 cm^{-1} in before-spectrum, are reduced to small peaks respectively at 2337 cm^{-1} and 1018 cm^{-1} after adsorption of Cd^{2+} and Hg^{2+} [23]. Various peaks at 912, 779, 686 and 537 cm^{-1} pertain

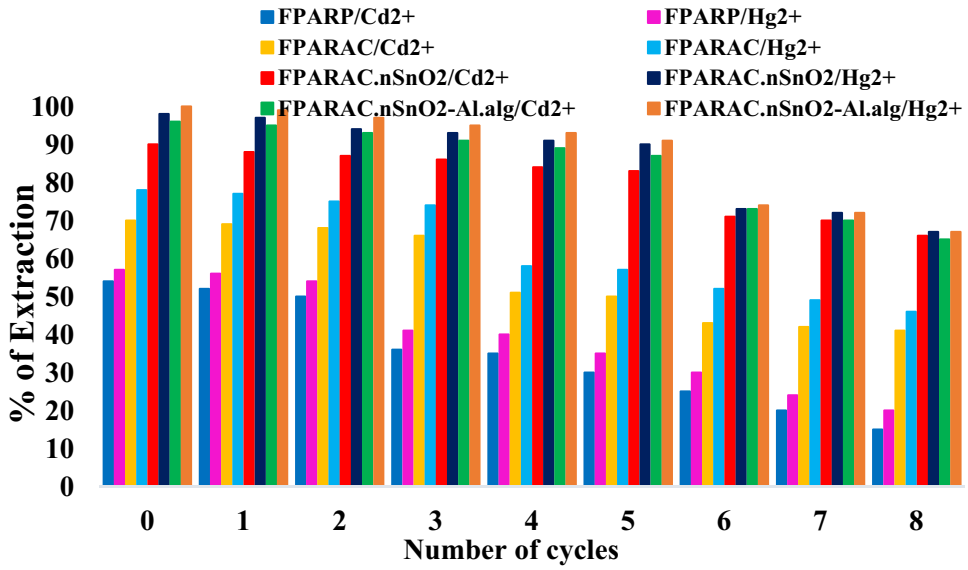

Fig. 11 Regeneration study of adsorbents

Table 2 Particle size calculation

2θ	θ	Radians	Cos θ				B	$L=\frac{k\lambda}{BCos\theta}$
26.63	13.315	0.232347	0.973129	26.525	26.732	0.207	0.003612	41.19853
33.91	16.955	0.295865	0.95655	33.808	34.042	0.234	0.004083	37.07649
37.98	18.99	0.331376	0.945596	37.89	38.125	0.235	0.004101	37.34642
51.82	25.91	0.45213	0.899519	51.71	51.991	0.281	0.004903	32.83264
54.81	27.405	0.478217	0.887817	54.685	54.975	0.29	0.00506	32.23302
57.96	28.98	0.505701	0.874835	57.74	58.063	0.323	0.005636	29.3693
61.91	30.955	0.540165	0.857624	61.806	62.135	0.329	0.005741	29.41234
64.75	32.375	0.564944	0.844619	64.652	65.012	0.36	0.006282	27.29349
65.99	32.995	0.575763	0.838777	65.867	66.242	0.375	0.006544	26.38423
71.37	35.685	0.622703	0.812305	71.17	71.57	0.4	0.00698	25.54132
78.76	39.38	0.687181	0.773037	78.607	79.026	0.419	0.007312	25.62169
Average:								31.301 nm

to bending vibrations of various functional groups in before-adsorption spectrum, are either disappeared or reduced in their intensities with little shift in their positions, indicative of sorption of metal ions [27]. New bands pertain to ester formation (1601 and 1163 cm^{-1}), 'Cd–O' and/or 'Hg–O–' (602, 449, 479 and 408 cm^{-1}) have appeared in the after-adsorption spectrum, indicating the interaction between the 'functional groups' of the adsorbent and Cd^{2+} and Hg^{2+} ions [27].

The FTIR spectrum of FPARAC, Fig. 4B, has the peaks at 3496–3095 cm^{-1} (broad, –OH, indicative of '–O···H···O' bonding); twin peaks at 2989 and 2916 cm^{-1} (strong, symmetric and asymmetric stretching of $–CH_2$) [30]; 2338 cm^{-1} (intensive, conjugated system), 1600 cm^{-1} (ester); 1441, 1407 and 1389 (small, aromatic nature), 938, 671, 597 and 498 cm^{-1} (varying intensities, bending vibrations) [28, 29]. After adsorption of Cd^{2+} and Hg^{2+}, there are marked variations, Fig. 4B: broad band of '–OH' stretching has disappeared; the twin bands of $–CH_2$ almost disappeared; and emphatic peak of conjugated system and peak of '–O–C' have been reduced. Further, new peaks of varying intensities due to defamations of metal (Cd/Hg)–O-are appeared at: 606, 598, 497, 458, 408 and 401 cm^{-1} [27]. These features indicate the formation of surface complex between Cd^{2+}/Hg^{2+} with various functional groups present in FPARAC.

When $nSnO_2$ is loaded on active carbon, FPARAC.$nSnO_2$, the active carbon spectrum, has been drastically changed, Fig. 4C. "Metal–O" stretchings generally appear below 1000 cm^{-1} [28]. In the present instance, a broad emphatic peak extending from 752 to 477 cm^{-1} with sharp shoot outs at: 611, 507 and 477 cm^{-1}, have appeared and further, some other new peaks appeared at 489, 434 and 425 cm^{-1}. These change in feature between FPARAC and FPARAC.$nSnO_2$ are indicative of surface modifications caused by $nSnO_2$ on FPARAC. After adsorption of Cd^{2+} and Hg^{2+} ions on FPARAC.$nSnO_2$, there are marked

changes in the spectral features: multiple small sharp peaks of '–NH/–OH' have changed to sharp multiple peaks (clear peak at 3745 cm^{-1}) with shift in their positions; twin peaks of $–CH_2$ stretchings at 2984 and 2891 cm^{-1} have almost disappeared [30]; 2340 cm^{-1} peak of 'conjugate system' has been reduced to small peaks with two shoots at: 2357 and 2330 cm^{-1} [28]; the ester peak at 1597 cm^{-1} has been changed to 1517 cm^{-1} with the reduction of intensity [29]; clear changes are observed in aromatic peaks (1448, 1407 and 1309 cm^{-1}); new peaks appeared at 609, 609, 605, 503, 477 and 404 cm^{-1} and they may be attributed to stretching of 'Cd/Hg–O' and/or '–O–Cd/Hg–O–' [27]. These changes in spectral characteristic indicate the adsorption of Cd^{2+}/Hg^{2+} on to the surface of FPARAC.nSnO_2.

On comparison of spectral characteristics of FPARAC.nSnO_2, Fig. 4C, with FPARAC.nSnO_2-Al.alg, Fig. 4D, marked difference can be observed, which are attributed to modification done by Al-alginate beads on the surface nature of FPARAC.nSnO_2-Al.alg. The clear changes observed are: a wide peak from 3605 to 3096 cm^{-1} (due to involvement '–OH/–NH–' groups in the hydrogen bond formation) [28]; strong peak of conjugate system at: 2353 cm^{-1} [28]; small peaks at: 1710, 1691 and 1585 cm^{-1} of carbonyl and ester [28]; various peaks of "Metal (Sn/Al)–O–" of different intensities at 854, 668, 572, 497, 448, 420, 404 and 401 cm^{-1} [27].

The spectrum of FPARAC.nSnO_2-Al.alg, Fig. 4D, after adsorption of Cd^{2+} and Hg^{2+}, has shown marked differences: the broad peak of '–OH/–NH–' has changed to a sharp peak at: 3509 cm^{-1} [23]; CH_2-peaks almost disappeared; peak pertaining to 'conjugate system' reduced (2327 cm^{-1}) [23]; small peaks of carbonyl and ester groups are reduced to a clear single peak at: 1588 cm^{-1} [23]; 1155 and 1024 peaks of '–C–O–/–O–C–O– ' are reduced to a single peak at 1044 cm^{-1} [23]; many vibrational frequencies of 'Metal (Sn/Al/Cd/Hg)–O–' are changed or disappeared. These changes in the spectral features indicate the formation of surface complex between Cd^{2+}/Hg^{2+} ions and various functional groups of the beads.

FESEM Analysis

Of the adsorbents investigated, FPARAC.nSnO_2-Al.alg beads were found to be highly effective in simultaneously removing Cd^{2+} and Hg^{2+} ions from contaminated water. Hence, FESEM images of FPARAC.nSnO_2-Al.alg beads were noted before and after adsorption of Cd^{2+} and Hg^{2+} ions and presented in Fig. 5A and B. In the before-adsorption image, Fig. 5A, many voids, sharp edges, and corners were noticed. In the after-adsorption image, Fig. 5B, there are emphatic morphological changes: some voids are missing or reduced, reduction in corers and edges.

Relatively homogenous features are appeared on the surface morphology of the image taken after adsorption. These changes in the morphological features are attributed to the adsorption of Cd^{2+} and Hg^{2+}.

Adsorption Parameters

Adsorption experiments were conducted by the batch adsorption process by varying different parameters including pH, adsorbent dosage, contact time and initial concentration of adsorbate ions to find optimum conditions for the simultaneous removal of cadmium and mercury ions from aqueous solutions with the adsorbents namely: FPARP, FPARAC, FPARAC.nSnO_2 and FPARAC.nSnO_2-Al.alg.

Effect of Initial pH

The effect of initial pH of the solution on the adsorption of cadmium and mercury ions were investigated by varying the pH from 1 to 10 and the results were shown in Fig. 6A. The maximum percentage removal was observed at pH: 6 for FPARP, pH: 5 for FPARAC, FPARAC.nSnO_2 and FPARAC.nSnO_2-Al.alg for both the metal ions, cadmium and mercury. The pHzpc values for the adsorbents were evaluated as per the standard methods described elsewhere and were presented in Fig. 6B [24]. The values were 5.5 for FPARP; 4.5 for FPARAC, FPARAC.nSnO_2 and for FPARAC.nSnO_2-Al.alg. At these pH_{ZPC} values, the surfaces of the adsorbents are neutral.

When the solution pH < pHpzc, the surface functional groups of the adsorbents were readily protonated, resulting electrostatic repulsion with metal cations in the solution and decreases the adsorption. At low pH values, H^+ ions compete with Cd^{2+}/Hg^{2+} ions, leading to low adsorption of Cd^{2+}/Hg^{2+} ions 'onto' the active sites of the adsorbent.

When the solution pH > pHzpc, the surface functional groups of the adsorbents were deprotonated, and the surface is charged negatively. At pH values above 6.5, the predominant species of cadmium and mercury ions are: Hg $(OH)_2$ or $HgCl_4^{2-}$; $[Cd(OH)_4]^-$ [21, 31]. Hence, at high pHs, the negatively charged surface of the adsorbents repels the cadmium and mercury species, resulting decrease in adsorption [5, 32].

Thus, good adsorption for both the ions are observed only when the solution pH values are around pHzpc. With increase or decrease in pH of the solution (than the value of pHzpc), the adsorption is decreased. At these pH values i.e. between 5 and 6, cadmium exists as Cd^{2+} (with traces of $CdOH^+$) while mercury as Hg^{2+} or $Hg(OH)^+$ and there is a least competition with H^+ with the cations of cadmium and mercury [21, 31]. The good adsorption at pH: 6.0/5.0, indicates the formation of surface complex and/or ion-exchange between Cd^{2+}/Hg^{2+} with the functional groups of sorbents.

The same is supported by the thermodynamic data with high ΔH° values and FTIR investigations.

Effect of Adsorbent Dosage

The effect of adsorbent dosage on the extraction of cadmium and mercury by FPARP, FPARAC, FPARAC.nSnO_2 and FPARAC.nSnO_2-Al.alg was investigated and the results were shown in Fig. 6C. Adsorbents dose was varied from 0.25 to 3.25 g/L and equilibrated for: 120 min with FPARP/Cd^{2+}/Hg^{2+}; 90 min with FPARAC/Cd^{2+}/Hg^{2+}; 60 min with FPARAC.nSnO_2/Cd^{2+}/Hg^{2+} and 75 min with FPARAC.nSnO_2-Al.alg/Cd^{2+}/Hg^{2+}, at an initial concentration of Cd^{2+}: 20.0 mg/L and Hg^{2+}: 15.0 mg/L at a temperature of 30 ± 1 °C.

With increasing the adsorbents dosage, the concentration of the Cd^{2+}, Hg^{2+} ions in the solution decreases. In other words, increasing the adsorbents dose significantly increased the Cd^{2+}, Hg^{2+} ions adsorptivity. On further increasing the adsorbents dose, a steady state was attained at 2.0 g/L for FPARP/Cd^{2+}/Hg^{2+}; 1.75 g/L for FPARAC/Cd^{2+}/Hg^{2+} and 1.5 g/L for both FPARAC.nSnO_2/ Cd^{2+}/Hg^{2+} and FPARAC.nSnO_2-Al.alg/Cd^{2+}/Hg^{2+}.

As already reported in literature, the increase in percent removal of adsorbate with increasing adsorbent dose could be attributed to the availability of more fresh active sites on the adsorbent surface for adsorption [24, 25, 33]. Increasing in adsorbents dose leads to increase in active sites of metal binding which means more metal ions are adsorbed. Hence, the percent removal increases till a steady state (saturation) is reached. On further addition of the adsorbents beyond the above said amounts, there is no significant change in the percent removal of metal ions. This can be attributed to the fact that the adsorbent gets aggregated and hence less effective surface area available for metal ions adsorption. The similar results were noticed in the previous works reported in the literature [23].

Effect of Contact Time

In the adsorption process, contact time is one of the important parameters. The effect of contact time on percent removal was investigated at various contact times in between 10 and 180 min, while maintaining all other parameters at optimum conditions. The results were shown in Fig. 6D.

The adsorption efficiency of the FPARP, FPARAC, FPARAC.nSnO_2 and FPARAC.nSnO_2-Al.alg towards Cd^{2+} and Hg^{2+} ions was very rapid in the initial stage of adsorption and slow down with time and attained a 'stead state' after certain equilibration time.

Initially, the surface of the adsorbents is endowed with more number of 'free active sites/ion', so the adsorption speed is fast at the beginning. With progress of equilibration time, the availability of active sited is decreed progressively in view of the fact that the dosage of adsorbent is fixed and consequently, only a fixed number of active sites are available. After certain equilibration time all the active sites are used-up, resulting a steady state: after 120 min with FPARP/Cd^{2+}/Hg^{2+}; 90 min with FPARAC/Cd^{2+}/Hg^{2+}; 60 min with FPARAC.nSnO_2/Cd^{2+}/Hg^{2+} and 75 min with FPARAC.nSnO_2-Al.alg/Cd^{2+}/Hg^{2+} [32, 34].

Effect of Initial Cd^{2+} and Hg^{2+} Concentrations

Different concentrations of Cd^{2+} and Hg^{2+} solutions in between 5.0 to 50.0 mg/L were examined to determine the efficiency of cadmium and mercury adsorption onto FPARP, FPARAC, FPARAC.nSnO_2 and FPARAC.nSnO_2-Al.alg. The other experimental parameters were maintained at optimum conditions. The results were shown in Fig. 6E and F.

As it can be seen from the Fig. 6E, the percent removal of Cd^{2+} and Hg^{2+} ions were decreased with increasing in the initial concentrations of the solutions. This might be due to the larger number of metal ions in the solution than the number of surface-active groups on the adsorbent. Hence, the fixed amounts of adsorbents will not continue to adsorb at the higher concentrations [23, 24, 31, 32].

As it can be seen from the Fig. 6F, the adsorption capacities of the adsorbents, qe, were increased with increasing in the initial concentrations of Hg^{2+} and Cd^{2+} solutions. At low concentrations, the ratio of the metal ions concentration to the surface area of the adsorbent was low while at higher concentrations, the active sites were completely occupied by the metal ions. Hence, due to increased diffusion of the metal ions into the boundary layer leading to higher adsorption capacity [31, 32].

Interference of Co-ions

The interference of co-ions on the extraction of cadmium and mercury by FPARP, FPARAC, FPARAC.nSnO_2 and FPARAC.nSnO_2-Al.alg was studied. In this investigation, the common ions namely Ca^{2+}, Mg^{2+}, Al^{3+}, Zn^{2+}, Fe^{2+}, Cu^{2+}, fluoride, chloride, sulphate, nitrate, phosphate, and bicarbonate were added in twofold excess than the cadmium and mercury ions due to their common existence in natural waters as well as wastewater from industrial sources. The results were presented in Fig. 7A and B.

As it can be seen from the Fig., presence of the common co-ions shows marginal effect on the extraction of cadmium and mercury ions. The extent of influence on the extraction depends on various factors such as electro negativity, charge, size, polarizability, repulsive forces between the ions, etc. [35].

Table 3 Thermodynamic parameters

Adsorbent	ΔH° (kJ/mol)	ΔS° (J/mol)	ΔG° (kJ/mol)				R^2
			303	313	323	333	
FPARP/Cd^2	7.99	26.49	− 8.02	− 8.28	− 8.55	− 8.81	0.9980
FPARP/Hg^{2+}	8.34	28.35	− 8.58	− 8.87	− 9.15	− 9.43	0.9977
FPARAC/Cd^2	12.44	43.49	− 13.17	− 13.60	− 14.04	− 14.47	0.9514
FPARAC/Hg^{2+}	31.87	107.79	− 32.63	− 33.71	− 34.79	− 35.87	0.9718
FPARAC.nSnO_2/Cd^{2+}	50.03	175.66	− 53.17	− 54.93	− 56.69	− 58.44	0.9900
FPARAC.nSnO_2/Hg^2	50.14	178.93	− 54.16	− 55.95	− 57.74	− 59.53	0.9881
FPARAC.nSnO_2-Al.alg/Cd^{2+}	65.29	229.23	− 69.39	− 71.68	− 73.97	− 76.27	0.9491
FPARAC.nSnO_2-Al.alg/Hg^{2+}	59.79	212.46	− 64.31	− 66.44	− 68.56	− 70.69	0.9262

Effect of Temperature and Thermodynamics of Adsorption

The effect of temperature on the extraction of Cd^{2+} and Hg^{2+} ions by FPARP, FPARAC, FPARAC.nSnO_2 and FPARAC.nSnO_2-Al.alg was investigated by using temperature range 303 to 333 K at other optimum conditions. The results were presented in Fig. 8A.

As seen in Fig., with increase in temperature the adsorption of the metal ions onto the adsorbents also increased. This indicates that the interaction of metal ions with the surface-active sites of the adsorbents is an endothermic process. At high temperature, the movement of the metal ions increases due to increase in energy of the system. More diffusion of the metal ions towards the adsorbents surface and more adsorption sites are created to enable the metal ions to penetrate more into the matrix of adsorbents and thereby, acquiring access to the inner-layered active sites, resulting more adsorption [30, 36].

Thermodynamic parameters of adsorption such as change in standard Gibbs free energy (ΔG°), change in standard enthalpy (ΔH°) and change in standard entropy (ΔS°) were calculated from the following equations [25, 30]:

$$\Delta G^\circ = -RT \ln K_d$$

$$\ln K_d = \Delta S^\circ/R - \Delta H^\circ/RT$$

$$K_d = q_e/C_e \text{ and}$$

$$\Delta G^\circ = \Delta H^\circ - T\,\Delta S^\circ$$

where K_d = distribution coefficient; qe = adsorbed amount of Cd^{2+}/Hg^{2+}; Ce = equilibrium Cd^{2+}/Hg^{2+}concentration; T = temperature (K), R = gas constant. The van't Hof plot, $\ln K_d$ versus 1/T, was as shown in Fig. 8B and the results were presented in Table 3.

The negative ΔG° values at all temperatures indicate that the adsorption of Cd^{2+} and Hg^{2+} ions by FPARP, FPARAC, FPARAC.nSnO_2 and FPARAC.nSnO_2-Al.alg was a spontaneous process. The positive values for the change in enthalpy, ΔH°, indicate the endothermic nature of adsorption of cadmium and mercury. Further, the high values of ΔH° suggest the mechanism of adsorption is 'ion-exchange and/or complex formation' between metal ions and adsorbents functional groups, as supported by FTIR-data. The positive ΔS^o values show the good affinity of the adsorbents for the metal ions. This results in increase in the metal ions concentration at the solid–liquid interface i.e. randomness in the system increases [15]. This is a favourable condition for metal ions to cross the interface barrier, resulting good sorption [37, 38]. The similar results were observed in the simultaneous extraction of lead and cadmium from contaminated water [23].

Adsorption Isotherms

In order to describe the interaction between the adsorbents and adsorbate ions at equilibrium, and to estimate the adsorption capacity, adsorption isotherms have been studied. The most common four different isotherms, Freundlich, Langmuir, Temkin and Dubinin–Radushkevich (D–R) were used to analyze the adsorption data [39–42]. Freundlich isotherm describes the multilayer adsorption of adsorbate ions on the heterogeneous surface of sorbents [15]. Langmuir adsorption isotherm is based on monolayer adsorption of metal ions on the homogeneous surface of adsorbents [15]. The separation factor, R_L, is a dimensionless parameter and specifies the feasibility of the adsorption process. As per Hall et al. the process is either unfavorable ($R_L > 1$), linear ($R_L = 1$), favorable ($0 < R_L < 1$) or irreversible ($R_L = 0$) [43]. The D-R isotherm is used to explain the heterogeneity of the adsorbent surface. Adsorption energy, E, is calculated based on D–R isotherm. Temkin isotherm studied the heat of adsorption and the adsorbent-adsorbate interaction of surfaces. Furthermore, the isotherms assume that the heat of adsorption, B, of all molecules in the layer decreased

Table 4 Evaluated adsorption isothermal parameters

Adsorbent/adsorbate	Parameter	Freundlich	Langmuir	Temkin	D-R isotherm
FPARP	Slope	0.3158	0.1757	1.1634	− 6.979E−7
Cd^{2+} removal	Intercept	0.7765	0.1353	2.1490	1.7283
	R^2	0.6945	0.9629	0.6866	0.8952
		1/n = 0.3158	R_L = 0.0371	B = 1.1634	E = 0.8464 kJ/mol
FPARP	Slope	0.2739	0.1988	0.9492	− 5.1567E−7
	Intercept	0.8021	0.0328	2.2678	2.2030
Hg^{2+} removal	R^2	0.6731	0.9636	0.6342	0.8369
		1/n = 0.2739	R_L = 0.0101	B = 0.9495	E = 0.9847 kJ/mol
FPARAC	Slope	0.3356	0.0986	2.0325	− 1.9942E−7
	Intercept	1.3447	0.0947	4.0821	2.2030
	R^2	0.8542	0.9636	0.8483	0.7925
Cd^{2+} removal		1/n = 0.3356	R_L = 0.0458	B = 2.0325	E = 1.5834 kJ/mol
FPARAC	Slope	0.2903	0.1008	1.7301	− 1.2976E−7
	Intercept	1.4469	0.0804	4.6772	2.1845
Hg^{2+} removal	R^2	0.8586	0.9904	0.8790	0.8184
		1/n = 0.2903	R_L = 0.0505	B = 1.7301	$R_{L=}$ 1.9629 kJ/mol
FPARAC.nSnO_2	Slope	0.2199	0.0492	3.1554	− 1.0329E−7
	Intercept	2.3639	0.0426	10.5245	2.8414
Cd^{2+} removal	R^2	0.9931	0.9910	0.9824	0.6980
		1/n = 0.2199	R_L = 0.0415	B = 3.1554	E = 2.2001 kJ/mol
FPARAC.nSnO_2	Slope	0.1431	0.0567	1.9147	− 3.5031E−8
Hg^{2+} removal	Intercept	2.4225	0.0336	11.4002	2.7430
	R^2	0.9677	0.9960	0.9435	0.5817
		1/n = 0.1431	R_L = 0.0380	B = 1.9147	E = 3.7779 kJ/mol
FPARAC.nSnO_2-Al.alg	Slope	0.1074	0.0562	1.6879	− 8.4796E−8
	Intercept	2.6242	6.8009	13.8470	2.8833
Cd^{2+} removal	R^2	0.7091	0.9932	0.6847	0.7453
		1/n = 0.1074	R_L = 0.8582	B = 1.6879	E = 2.4283 kJ/mol
FPARAC.nSnO_2-Al.alg	Slope	0.2028	0.050	3.2259	− 2.8960E−7
	Intercept	2.4038	0.0337	10.3727	2.8960
Hg^{2+} removal	R^2	0.9925	0.9902	0.9860	0.6998
		1/n = 0.2028	R_L = 0.0430	B = 3.5529	E = 1.3139 kJ/mol

linearly by increasing the coverage during adsorption process [4, 25, 36, 44].

The plots of these isotherms and the evaluated factors were depicted in Fig. 9A–D and Table 4. The correlation coefficient (R^2) values were used to select a best adsorption model that fits the experimental data. The R^2 values close to unity denotes that the model fits the data well [22, 36].

As it can be seen from the Table, higher R^2 values (close to 1) for the Langmuir plots compared with other models showed better fit to the experimental data. According to the Langmuir, the simultaneous adsorption of Cd^{2+} and Hg^{2+} ions 'onto' the adsorbents occurs in homogeneous surface sites. Further, the positive values of the separation factors (R_L) were within the range of 0 to 1 indicate that the adsorption process is favorable 'onto' adsorbents. While on the other hand, R^2 values of FPARAC.nSnO_2/Cd^{2+} and FPARAC.nSnO_2-Al.alg/Hg^{2+}, were higher (close to 1) for the Freundlich plot than the Langmuir plot. Furthermore, the values of 1/n were > 1 for these adsorbents, which reveals that the cadmium and mercury adsorption onto FPARAC.nSnO_2 and FPARAC.nSnO_2-Al.alg, respectively, is favorable and heterogeneous. The heat of adsorption (B) and the adsorption energy, E, values were calculated using Temkin and Dubinin–Radushkevich equations.

Adsorption Kinetics

Adsorption kinetics describes time required for the adsorption process and the adsorption rate of adsorbate by the adsorbent. In the present study, four kinetic

Table 5 Evaluated adsorption kinetical parameters

Adsorbent/adsorbate	Parameter	Pseudo-first order	Pseudo-second order	Elovich model	Bangham's pore diffusion
FPARP	Slope	−0.011	0.0967	1.836	0.8390
Cd^{2+} removal	Intercept	0.8211	1.592	−4.28	−2.3266
	R^2	0.9801	0.9875	0.9783	0.9502
FPARP	Slope	−0.013	0.1578	1.42	0.7921
Hg^{2+} removal	Intercept	0.7941	13.88	−3.148	−2.1771
	R^2	0.8993	0.9383	0.9697	0.9440
FPARAC	Slope	−0.087	0.1034	2.268	0.6546
Cd^{2+} removal	Intercept	3.536	4.0541	−3.523	−1.7079
	R^2	0.6570	0.9802	0.9398	0.9016
FPARAC	Slope	−0.084	0.1164	2.0264	0.7416
Hg^{2+} removal	Intercept	3.3682	5.224	−3.416	−1.779
	R^2	0.6700	0.9789	0.9499	0.9300
FPARAC.nSnO_2	Slope	−0.031	0.0737	2.98	0.6957
Cd^{2+} removal	Intercept	1.4295	1.701	−2.669	−1.499
	R^2	0.9057	0.9680	0.7637	0.7650
FPARAC.nSnO_2	Slope	−0.036	0.0987	2.135	0.6657
Hg^{2+} removal	Intercept	1.4068	1.778	−1.222	−1.388
	R^2	0.8820	0.9722	0.7058	0.7105
FPARAC.nSnO_2−Al.alg	Slope	−0.022	0.0724	2.877	0.6812
Cd^{2+} removal	Intercept	1.2463	1.347	−1.667	−1.4025
	R^2	0.9745	0.9860	0.8175	0.8395
FPARAC.nSnO_2-Al.alg	Slope	−0.023	0.0967	2.092	0.6688
Hg^{2+} removal	Intercept	1.1011	1.592	−0.7970	−1.3507
	R^2	0.9930	0.9875	0.7921	0.8242

models namely, pseudo-first and second order equations, Elovich model and Bangham's pore diffusion model were employed [45–48]. The pseudo first-order model is used to describe the adsorption of liquid adsorbate ions 'onto' the solid adsorbent at different time intervals. The pseudo-second order model is based on the assumption that the adsorption involving valence forces through sharing of electrons between adsorbate and adsorbent. Elovich kinetic model is applied for the adsorption of solutes from a liquid solution. Bangham's pore diffusion model is used to describe pore diffusion during adsorption process. The correlation coefficient (R^2) values were used to confirm the favoured adsorption kinetic model. Higher the correlation coefficient (R^2) values (close to 1), greater will be the linearity. This confirmed the best fit kinetic model to the experimental data. The plots of these kinetics and the evaluated factors were depicted in Fig. 10A–D and Table 5.

As it can be seen from the Table, the R^2 values for the adsorption kinetics of the metal ions were higher (close to 1) for the pseudo-second order model compared to other models. Hence, the pseudo-second order model is a best model fitting the kinetics of the adsorption of the metal ions, cadmium and mercury. Thus, the rate determining step may be the chemisorption process and it requires the interchange or involvement of electrons. While on the other hand, the adsorption kinetics of Hg^{2+} ions by FPARAC were best fitted with Elovich model ($R^2 = 0.9697$) and Hg^{2+} ions by FPARAC.nSnO_2-Al.alg was best fitted with pseudo-first order model ($R^2 = 0.9930$).

Simultaneous Extraction of Cadmium and Mercury Ions

The optimum extraction conditions for the maximum removal of individual cadmium and mercury ions by FPARP, FPARAC, FPARAC.nSnO_2 and FPARAC.nSnO_2-Al.alg at an initial concentration of Cd^{2+} (20.0 mg/L) and Hg^{2+} (15.0 mg/L) are: pH: 6.0, equilibration time: 120 min, adsorbent dosage: 2.0 g/L for FPARP/Cd^{2+}/Hg^{2+}; pH: 5.0, equilibration time: 90 min, adsorbent dosage: 1.75 g/L for

Table 6 Simultaneous removal of cadmium and mercury ions

Samples	Concentration of mixture mercury + cadmium (mg/L)		After adsorption mg/L		% Removal	
	Cd^{2+}	Hg^{2+}	Cd^{2+}	Hg^{2+}	Cd^{2+}	Hg^{2+}
A: FPARP: Optimum conditions: pH: 6.0; dosage: 2.50 g/L; contact time: 130 min; rpm: 350; Temp.: 30 ± 1 °C						
1	2.0	1.0	0	0	100	100
2	2.5	1.5	0	0	100	100
3	3.0	2.0	0	0	100	100
4	3.5	2.5	0	0	100	100
5	4.0	3.0	0	0	100	100
B: FPARAC: Optimum conditions: pH: 5.0; dosage: 2.0 g/L; contact time: 100 min; rpm: 350; Temp.: 30 ± 1 °C						
1	2.0	1.0	0	0	100	100
2	2.5	1.5	0	0	100	100
3	3.0	2.0	0	0	100	100
4	3.5	2.5	0	0	100	100
5	4.0	3.0	0	0	100	100
C: FPARAC.nSnO_2: Optimum conditions: pH: 5.0; dosage: 1.75 g/L; contact time: 70 min; rpm: 350; Temp.: 30 ± 1 °C						
1	2.0	1.0	0	0	100	100
2	2.5	1.5	0	0	100	100
3	3.0	2.0	0	0	100	100
4	3.5	2.5	0	0	100	100
5	4.0	3.0	0	0	100	100
D: FPARAC.nSnO_2-Al.alg: Optimum conditions: pH: 5.0; dosage: 1.75 g/L; contact time: 80 min; rpm: 350; Temp.: 30 ± 1 °C						
1	2.1	4.2	0	0	100	100
2	2.9	5.1	0	0	100	100
3	3.4	6.5	0	0	100	100
4	4.1	7.8	0	0	100	100
5	4.8	8.6	0	0	100	100

The values are average of five estimations; S.D.: ± 0.18

FPARAC/Cd^{2+}/Hg^{2+}; pH: 5.0, equilibration time: 60 min, adsorbent dosage: 1.5 g/L for FPARAC.nSnO_2/Cd^{2+}/Hg^{2+} and pH: 5.0, equilibration time: 75 min, adsorbent dosage: 1.5 g/L for FPARAC.nSnO_2-Al.alg/Cd^{2+}/Hg^{2+} at a temperature of 30 ± 1 °C.

Hence, the simultaneous extraction of both the metal ions, cadmium, and mercury, was also investigated at the above said pH values with the adsorbents. Results were noted in Table 6. The results revealed that except two extraction parameters, dosages of adsorbents and equilibration times, both the metal ions were effectively removed at the established extraction conditions. All other parameters were remained constant except these two parameters. There was a small increase in dosages of adsorbents and equilibration times. The adsorbent dosage and equilibration time respectively needed were found to be 2.50 g/L, 130 min for FPARP/Cd^{2+}/Hg^{2+}; 2.0 g/L, 100 min for FPARAC/Cd^{2+}/Hg^{2+} and 1.75 g/L; 70 min for FPARAC.nSnO_2/Cd^{2+}/Hg^{2+} and 1.75 g/L, 80 min for FPARAC.nSnO_2-Al.alg/Cd^{2+}/Hg^{2+}.

Regeneration and Reuse of Spent Adsorbents

Regeneration and reusability of the spent adsorbents are important considerations from the economic point of view. To investigate the recycling ability of the adsorbents, FPARP, FPARAC, FPARAC.nSnO_2 and FPARAC.nSnO_2-Al.alg, the regeneration studies were conducted with the metal ions solution having 20.0 mg/L of Cd^{2+} and 15.0 mg/L of Hg^{2+}. Various solutions comprising of acids, bases and salts and their blends at different concentrations, were tried to regenerate the spent sorbents. 0.1 N HCl was effective in regenerating the spent adsorbents [25].

Overnight incubation of the Cd^{2+}/Hg^{2+} loaded adsorbents into 0.01 N HCl solution followed by filtering and dried at 105 °C were done to complete the regeneration process. Now, the adsorbents were re-used for the extraction of Cd^{2+} and Hg^{2+} ions. Results were presented in Fig. 11. The results revealed that no significant changes in the percent removal up to 5-cycles for FPARAC.nSnO_2 and FPARAC.

$nSnO_2$-Al.alg, up to 3-cycles for FPARAC and up to 2-cycles of adsorption–desorption for FPARP. Marginally declined removal efficiencies could be observed.

The decrease in adsorption with the increases in number of cycles of regeneration-cum-reuse, may be due to loss and/or non-generation of active sites on the adsorbent's surface. Some of the active sites may be destroyed during the treatment process [25].

Hence, the cost-effective synthesis, higher adsorption capacity and good regeneration efficiency of the adsorbents, FPARP, FPARAC, FPARAC.$nSnO_2$ and FPARAC.$nSnO_2$-Al.alg, makes them as good sorbents in wastewater treatment.

Applications

The simultaneous removal of Cd^{2+} and Hg^{2+} ions was also investigated at an environmental level to treat real industrial wastewater samples collected from battery and electroplating industries in Madras and Hyderabad, India. The adsorbents developed in the present study, FPARP, FPARAC, FPARAC.$nSnO_2$ and FPARAC.$nSnO_2$-Al.alg, were used to treat industrial effluents. The samples were treated at the optimum conditions of extraction investigated in the present study: pH: 6.0, equilibration time: 130 min, adsorbent dosage: 2.5 g/L for FPARP/Cd^{2+}/Hg^{2+}; pH: 5.0, equilibration time: 100 min, adsorbent dosage: 2.0 g/L for FPARAC/Cd^{2+}/Hg^{2+}; pH: 5.0, equilibration time: 70 min, adsorbent dosage: 1.75 g/L for FPARAC.$nSnO_2$/Cd^{2+}/Hg^{2+} and pH: 5.0, equilibration time: 80 min, adsorbent dosage: 1.75 g/L for FPARAC.$nSnO_2$-Al.alg/Cd^{2+}/Hg^{2+} at a temperature of 30 ± 1 °C. The results were presented in Table 7.

The results show the complete removal efficiency of Cd^{2+} and Hg^{2+}ions onto adsorbents at the said extraction conditions. Hence, these adsorbents could remove effectively both Cd^{2+} and Hg^{2+} ions from industrial effluents simultaneously.

Comparison with Other Reported Adsorbents

The adsorption performances of developed adsorbents in this investigation, FPARP, FPARAC, FPARAC.$nSnO_2$ and FPARAC.$nSnO_2$-Al.alg, were compared with those of previously reported adsorbents. The results were presented in Table 8. These previous reports pertain to the removal of individual Cd^{2+} and Hg^{2+} from water. The main merit of the present sorbents is that they are effective in removing simultaneously the cadmium and mercury ions from contaminated waters.

As is evident from the Table 8, all the adsorbents have good sorption capacities for cadmium and mercury ions. The results show the adsorbents have better adsorption capacity than the many other reported adsorbents. Hence, these adsorbents have high potential for the simultaneous removal of Cd^{2+} and Hg^{2+} ions from wastewater.

Table 7 Applications (Optimum conditions: FPARP-pH: 6.0, equilibration time: 130 min, adsorbent dosage: 2.5 g/L; FPARAC-pH: 5.0, equilibration time: 100 min, adsorbent dosage: 2.0 g/L; FPARAC.$nSnO_2$-pH: 5.0, equilibration time: 70 min, adsorbent dosage: 1.75 g/L and FPARAC.$nSnO_2$-Al.alg-pH: 5.0, equilibration time: 80 min, adsorbent dosage: 1.75 g/L at a temperature of 30 ± 1 °C)

Sample	C_i[a], in mg/L Cd^{2+}: Hg^{2+}	Cd^{2+} and Hg^{2+} ions removal							
		FPARP		FPARAC		FPARAC.$nSnO_2$		FPARAC.$nSnO_2$-Al.alg	
		Ce[a] mg/L	% extraction	Ce[a] mg/L	% extraction	Ce[a] mg/L	% extraction	Ce[a] mg/L	% extraction
A: Effluents of battery industries									
1	2.2: 1.5	0	100	0	100	0	100	0	100
2	2.6: 2.3	0	100	0	100	0	100	0	100
3	3.7: 2.1	0	100	0	100	0	100	0	100
4	4.1: 2.2	0	100	0	100	0	100	0	100
5	4.8: 2.7	0	100	0	100	0	100	0	100
B: Effluents of electro plating industry									
1	1.8: 1.0	0	100	0	100	0	100	0	100
2	2.1: 1.3	0	100	0	100	0	100	0	100
3	2.8: 1.7	0	100	0	100	0	100	0	100
4	3.4: 2.0	0	100	0	100	0	100	0	100
5	3.9: 2.4	0	100	0	100	0	100	0	100

Ci initial Cd^{2+}/Hg^{2+} concentrations in the effluents samples collected in the battery and electroplating industries, *Ce* equilibrium Cd^{2+}/Hg^{2+} concentrations after treating with FPARP, FPARAC, FPARAC.$nSnO_2$ and FPARAC.$nSnO_2$-Al.alg

[a]Mean of five determinations; SD: ± 0.23

Table 8 Comparison of adsorbents

S. no.	Sorbent	pH	pollutant	Adsorbent capacity (mg/g)	References
1	Modified Fe oxide	.	Mercury	0.59	[49]
2	Fe–Sn–MnOx	.	Mercury	3.75	[50]
3	Green coconut shell	5.0	Cadmium	11.96	[51]
4	Succinic anhydride modified apple pomace	4.0	Cadmium	4.45	[52]
5	Activated carbon prepared from African palm fruit	8.0	Cadmium	1.82	[53]
6	palm oil fuel ash	7.0	Mercury	0.99	[54]
7	SBZ-Chemical activation using $ZnCl_2$	6.0	Mercury	11.5	[22]
8	Brewed tea waste	4.0	Cadmium	2.468	[55]
9	Hickory chips biochar	6.0	Mercury	5.0	[56]
10	Coconut activated carbon	7.0	Mercury	5.2	[57]
11	Microwaved olive stone activated carbon	5.0	Cadmium	11.7	[58]
12	Soybean stalk	7.0	Mercury	0.67	[59]
13	Natural biosorbent and activated carbon	4.0	Cadmium	0.08	[60]
14	Phragmites karka	7.0	Mercury	2.3	[61]
15	Granular activated carbon and activated clay	6.0	Cadmium	9.65	[62]
16	Corn straw	6.0	Mercury	5.1	[63]
17	Garlic (*Allium sativum* L.)	…	Mercury	0.6	[64]
18	S-MWCNT4060	7.0	Mercury	0.7	[65]
19	New low-cost adsorbent bamboo charcoal	8.0	Cadmium	12.08	[66]
20	FPARP	6.0	Cadmium	5.25	Present work
21	FPARP	6.0	Mercury	4.9	
22	FPARAC	5.0	Cadmium	8.74	
23	FPARAC	5.0	Mercury	7.98	
24	FPARAC.nSnO_2	5.0	Cadmium	14.18	
25	FPARAC.nSnO_2	5.0	Mercury	9.8	
26	FPARAC.nSnO_2-Al.alg	5.0	Cadmium	12.8	
27	FPARAC.nSnO_2-Al.alg	5.0	Mercury	10.0	

Conclusions

Ficus Panda areal roots powder (FPARP) and its active carbon (FPARAC) are identified to have affinity for Cd^{2+} and Hg^{2+}. Nano SnO_2 particles of average size: 31.3 nm are successfully synthesized by new green methods adopting *aloe-vera* gel as capping agent. By doping these green synthesized nSnO_2 in the matrix of the active carbon (FPARAC.nSnO_2), the adsorption nature towards the said cations is further increased. To prevent 'agglomeration' of nanoparticles and make filtration easy, the composite of 'active carbon and nSnO_2' are embedded in Al-alginate beads (FPARAC.nSnO_2-Al.alg). Thus, FPARP, FPARAC, 'FPARAC + nSnO_2' and 'FPARAC.nSnO_2-Al.alg', are investigated as adsorbents for the removal of Cd^{2+} and Hg^{2+} ions.

The adsorbents are characterized by various methods including XRD, FTIR and FESEM analysis. Various extraction conditions are optimized for the simultaneous extraction of cadmium and mercury ions from wastewater adopting batch methods. The beads have exhibited good sorption capacities as high as: 12.8 mg/g for Cd^{2+} and 10.0 mg/g for Hg^{2+} at pH: 5 and equilibration time of 80 min. The effects of co-ions on the adsorptivities are also investigated. The regeneration and reuse of spent adsorbents are investigated and observed that no significant changes in the percent removal up to 5-cycles for 'FPARAC.nSnO_2' and 'FPARAC.nSnO_2-Al.alg', 3-cycles for 'FPARAC' and 2-cycles for 'FPARP'.

The adsorption nature is analyzed by adopting various isotherm and kinetic models. Different thermodynamic parameters are evaluated and noted that the adsorption process is 'spontaneous' and 'endothermic' in nature. Thermodynamic studies and FTIR investigations suggest that the mechanism of adsorption is 'ion-exchange and/or complex formation' between metal ions and surface functional groups of the adsorbents. The developed methodologies are applied to treat real wastewater samples of industries. Thus, the inherent merits of active carbon of Ficus *Panda* areal roots, green synthesized nSnO_2 and Al-alginate beads are successfully explored for their

cumulative adsorption nature for the simultaneous removal of Cd^{2+} and Hg^{2+} ions. The striking merit of this investigation is that robust and eco-friendly adsorbents with high sorption capacities are developed for the extraction of both Cd^{2+} and Hg^{2+} ions from wastewater at nearly neutral pH conditions.

Acknowledgements The authors are thankful to Koneru Lakshmaiah Education Foundation, Guntur, Andhra Pradesh, for providing necessary facilities to pursue this research investigation.

Author Contributions KR: Concept development and guidance during the progress of this research work. MS, VSR and SM**:** are the Research Scholars contributed to the experimental part of this investigation, interpretation of the results and preparation of first draft of the manuscript. All authors read and approved the final manuscript.

Funding No Funding.

Data Availability All the date is available in the manuscript.

Declarations

Competing Interests On behalf of all authors, the corresponding author states that there are no conflict of interests.

Ethical Approval Not Applicable.

References

1. Xia M, Chen Z, Li Y, Li C, Ahmad NM, Cheema WA, Zhu S (2019) Removal of Hg(II) in aqueous solutions through physical and chemical adsorption principles. RSC Adv 9:20941–20953. https://doi.org/10.1039/c9ra01924c
2. Wołowiec M, Komorowska-Kaufman M, Pruss A, Rzepa G, Bajda T (2019) Removal of heavy metals and metalloids from water using drinking water treatment residuals as adsorbents: a review. Minerals 9(487):1–17. https://doi.org/10.3390/min9080487
3. Amandeep K, Sangeeta S (2017) Removal of Heavy metals from waste water by using various adsorbents-a review. Indian J Sci Technol. https://doi.org/10.17485/ijst/2017/v10i34/117269
4. Giwa AA, Bello IA, Oladipo MA, Adeoye DO (2013) Removal of cadmium from waste-water by adsorption using the husk of melon (*Citrullus lanatus*) seed. Int J Basic Appl Sci 2(1):110–123
5. Shaojun H, Chengzhang M, Yaozu L, Chungang M, Ping D, Yubo J (2016) Removal of mercury(II) from aqueous solutions by adsorption on poly (1-amino-5-chloroanthraquinone) nanofibrils: equilibrium, kinetics, and mechanism studies. J Nanomater. https://doi.org/10.1155/2016/7245829
6. Benettayeb A, Morsli A, Guibal E, Kessas R (2021) New derivatives of urea-grafted alginate for improving the sorption of mercury ions in aqueous solutions. Mater Res Express 8:035303. https://doi.org/10.1088/2053-1591/abeabc
7. Himanshu A, Divyanshi S, Susheel KS, Sonika T, Saiqa I (2010) Removal of mercury from wastewater use of green adsorbents—A review. EJEAFChe 9(9):1551–1558
8. Vinni Novi T, Vinoth Kumar V, Senthil Kumar P, Christy C, Sai Lavanyaa S, Vishnu D, Saravanan A, Vasanth Kumar V, Subramanian S (2016) Review on nanoadsorbents: a solution for heavy metal removal from wastewater. IET Nanobiotechnol. https://doi.org/10.1049/iet-nbt.2015.0114
9. Joseph KC, Fang Z, Sha C, Yong YC (2020) Green synthesis of Ag and Pd nanoparticles for water pollutants treatment. Water Sci Technol 82(11):2344–2352. https://doi.org/10.2166/wst.2020.498
10. Benettayeb A, Guibal E, Bhatnagar A, Morsli A, Kessas R (2021) Effective removal of nickel(II) and zinc(II) in mono-compound and binary systems from aqueous solutions by application of alginate-based materials. Int J Environ Anal Chem. https://doi.org/10.1080/03067319.2021.1887164
11. Suneetha M, SyamaSundar B, Ravindhranath K (2015) Removal of fluoride from polluted waters using active carbon derived from barks of *Vitex negundo* plant. J Anal Sci Technol 6:15. https://doi.org/10.1186/s40543-014-0042-1
12. Wang C, Wang H (2018) Carboxyl functionalized *Cinnamomum camphora* for removal of heavy metals from synthetic wastewater-contribution to sustainability in agroforestry. J Clean Prod. https://doi.org/10.1016/j.jclepro.2018.03.004
13. Benettayeb A, Haddou B (2021) New biosorbents based on the seeds, leaves and husks powder of *Moringa oleifera* for the efective removal of various toxic pollutants. Int J Environ Anal Chem 00:1–26. https://doi.org/10.1080/03067319.2021.1963714
14. Benettayeb A, Ghosh S, Usman M, Seihoub FZ, Sohoo I, Chia CH, Sillanpää M (2022) Some Well-known alginate and chitosan modifications used in adsorption: a review. Water 14:1353. https://doi.org/10.3390/w14091353
15. Benettayeb A, Usman M, Calvin Tinashe C, Adam T, Haddou B (2022) A critical review with emphasis on recent pieces of evidence of *Moringa oleifera* biosorption in water and wastewater treatment. Environ Sci Pollut Res 29:48185–48209. https://doi.org/10.1007/s11356-022-19938-w
16. American Public Health Association, APHA (1998) Standard methods for the examination of water and waste water. American Public Health Association, Washington, DC
17. Bureau of Indian Standards (1989) Activated carbon powdered and granular-methods of sampling and its tests, Bureau of Indian Standards, New Delhi, IS 877
18. American Society for Testing Materials (ASTM) (2006) Standard test method for determination of iodine number of activated carbon D4607-94, ASTM
19. Namasivayam C, Kadirvelu K (1997) Activated carbons prepared from coir pith by physical and chemical activation methods. Biores Technol 62(3):123–127. https://doi.org/10.1016/S0960-8524(97)00074-6
20. El-Hendawy AN, Samra SE, Girgis BS (2001) Adsorption characteristics of activated carbons obtained from corncobs. Colloids Surf A 180(3):209–221
21. Brunauer S, Emmett PH, Teller E (1938) Adsorption of gases in multimolecular layers. J Am Chem Soc 60(2):309–319. https://doi.org/10.1021/ja01269a023
22. Giraldo S, Robles I, Ramirez A, Florez E, Acelas N (2020) Mercury removal from wastewater using agroindustrial waste adsorbents. SN Appl Sci 2:1029. https://doi.org/10.1007/s42452-020-2736-x
23. Sneha Latha P, Biftu WK, Suneetha M, Ravindhranath K (2021) Simultaneous removal of Lead and Cadmium ions from simulant and industrial waste water: using *Calophyllum Inophyllum* plant materials as sorbents. Int J Phytoremediat. https://doi.org/10.1080/15226514.2021.1961121
24. Biftu WK, Sunetha M, Ravindhranath K (2021) Zirconium-alginate beads doped with H2SO4-activated carbon derived from leaves of *Magnoliaceae* plant as an effective adsorbent for the removal of chromate. Biomass Convers Biorefin. https://doi.org/10.1007/s13399-021-01568-w
25. Sneha Latha P, Biftu WK, Suneetha M, Ravindhranath K (2022) Adsorptive removal of toxic chromate and phosphate ions from

polluted water using green synthesized nano metal (Mn-Al-Fe) oxide. Biomass Convers Bioref. https://doi.org/10.1007/s13399-021-02293-0
26. Dorofeev GA, Streletskii AN, Povstugar IV, Protasov AV, Elsukov EP (2012) Determination of nanoparticle sizes by X-ray diffraction. Colloid J 74(6):675–685. https://doi.org/10.1134/S1061933X12060051
27. Sneha Latha P, Suneetha M, Ravindhranath K (2022) Novel adsorbents for simultaneous extraction of lead and cadmium ions from polluted water: based on active carbon, nanometal (Zr-Ce-Sm)-mixed oxides and iron-alginate beads. Biomass Convers Bioref. https://doi.org/10.1007/s13399-022-03063-2
28. Anil B, Suneetha M, Rafi SM, Ravindhranath K (2022) Simple bio-sorbents derived from *Mimusops elengi* plant for the effective removal of molybdate from industrial wastewater. Biomass Convers Bioref. https://doi.org/10.1007/s13399-022-02830-5
29. Leela Srinivas T, Suneetha M, Sneha Latha P, Biftu WK, Ravindhranath K (2022) Stem powder and its active carbon of *Arachis hypogaea* plant for lead (II) removal: application to treat battery-based industrial effluents. Int J Phytoremediat. https://doi.org/10.1080/15226514.2022.2095975
30. Mustapha S, Shuaib DT, Ndamitso MM, Etsuyankpa MB, Sumaila A, Mohammed UM, Nasirudeen MB (2019) Adsorption isotherm, kinetic and thermodynamic studies for the removal of Pb(II), Cd(II), Zn(II) and Cu(II) ions from aqueous solutions using *Albizia lebbeck* pods. Appl Water Sci 9:142. https://doi.org/10.1007/s13201-019-1021-x
31. Al-Ghouti MA, Daana D, Abu-Dieyeh M, Khraisheh M (2019) Adsorptive removal of mercury from water by adsorbents derived from date pits. Sci Rep 9:15327. https://doi.org/10.1038/s41598-019-51594-y
32. Liu Z, Sun Y, Xu X, Qu J, Qu B (2020) Adsorption of Hg(II) in an aqueous solution by activated carbon prepared from rice husk using KOH activation. ACS Omega 5:29231–29242. https://doi.org/10.1021/acsomega.0c03992
33. Suneetha M, Syama Sundar B, Ravindhranath K (2015) De-fluoridation of waters using low-cost HNO3 activated carbon derived from stems of *Senna occidentalis* plant. Int J Environ Technol Manag 18(5/6):420–447. https://doi.org/10.1504/IJETM.2015.073079
34. Suneetha M, Ravindhranath K (2017) Adsorption of nitrite ions from wastewater using bio-sorbents derived from *Azadirachta indica* plant. Asian J Water Environ Pollut 14(2):71–79. https://doi.org/10.3233/AJW-170017
35. Onyango MS, Kojima Y, Aoyi O, Bernardo EC, Matsuda H (2004) Adsorption equilibrium modeling and solution chemistry dependence of fluoride removal from water by trivalent-cation-exchanged zeolite F-9. J Colloid Interface Sci 279(2):341–350. https://doi.org/10.1016/j.jcis.2004.06.038
36. Batool F, Akbar J, Iqbal S, Noreen S, Bukhari SNA (2018) Study of isothermal, kinetic, and thermodynamic parameters for adsorption of cadmium: an overview of linear and nonlinear approach and error analysis. Bioinorg Chem Appl. https://doi.org/10.1155/2018/3463724
37. Huang X, Gao NY, Zhang QL (2007) Thermodynamics and kinetics of cadmium adsorption onto oxidized granular activated carbon. J Environ Sci 19(11):1287–1292. https://doi.org/10.1016/S1001-0742(07)60210-1
38. Sujitha R, Ravindhranath K (2018) Removal of lead (II) from wastewater using active carbon of *Caryota urens* seeds and its embedded calcium alginate beads as adsorbents. J Environ Chem Eng 6(4):4298–4309. https://doi.org/10.1016/j.jece.2018.06.033
39. Freundlich HM (1906) Over the adsorption in solution. J Phys Chem 57(385471):1100–1107
40. Langmuir I (1918) The adsorption of gases on plane surfaces of glass, mica and platinum. J Am Chem Soc 40(9):1361–1403. https://doi.org/10.1021/ja02242a004
41. Temkin MJ, Pyzhev V (1940) Recent modifications to Langmuir isotherms. Acta Physiochim USSR 12:217–222
42. Dubinin MM (1947) The equation of the characteristic curve of activated charcoal. Dokl Akad Nauk SSSR 55:327–329
43. Hall KR, Eagleton LC, Acrivos A, Vermeulen T (1966) Pore-and solid-difusion kinetics in fxed-bed adsorption under constantpattern conditions. Ind Eng Chem Fundam 5(2):212–223. https://doi.org/10.1021/i160018a011
44. Shivangi BS, Sarkar T (2021) Simultaneous removal of cadmium and lead ions from aqueous solutions by nickel oxide-decorated reduced graphene oxides. Int J Environ Sci Technol. https://doi.org/10.1007/s13762-021-03510-z
45. Aharoni C, Ungarish M (1977) Kinetics of activated chemisorption part 2 theoretical models. J Chem Soc Faraday Trans 73:456–464. https://doi.org/10.1039/F19777300456
46. Chien SH, Clayton WR (1980) Application of the Elovitch equation to the kinetics of phosphorus release and sorption in soils. Soil Sci Soc Am J 44:265–268
47. Ho YS, McKay G (1999) Pseudo-second order model for sorption processes. Process Biochem 34(5):451–465. https://doi.org/10.1007/s11356-019-05050
48. Lagergren S (1898) About the theory of so-called adsorption of soluble substances. Kungliga Sven Vetensk. Handlingar 24(4):1–39
49. Parham H, Zargar B, Shiralipour R (2012) Fast and efficient removal of mercury from water samples using magnetic iron oxide nanoparticles modified with 2-mercaptobenzothiazole. J Hazard Mater 205:94–100. https://doi.org/10.1016/j.jhazmat.2011.12.026
50. Xu H, Xie J, Ma Y, Qu Z, Zhao S, Chen W, Huang W, Yan N (2015) The cooperation of FeSn in a MnOx complex sorbent used for capturing elemental mercury. Fuel 140:803–809. https://doi.org/10.1016/j.fuel.2014.10.004
51. Sousa FW, Oliveira AG, Ribeiro JP, Rosa MF, Keukeleire D, Nascimento RF (2010) Green coconut shells applied as adsorbent for removal of toxic metal ions using fixed-bed column technology. J Environ Manage 91(8):1634–1640
52. Chand P, Shil AK, Sharma M, Pakade YB (2014) Improved adsorption of cadmium ions from aqueous solution using chemically modified apple pomace: mechanism, kinetics, and thermodynamics. Int Biodeterior Biodegradation 90:8–16
53. Abdulrazak S, Hussaini K, Sani HM (2017) Evaluation of removal efficiency of heavy metals by low-cost activated carbon prepared from African palm fruit. Appl Water Sci 7(6):3151–3155. https://doi.org/10.1007/s13201-016-0460-x
54. Imla Syafiqah MS, Yussof HW (2018) Kinetics, isotherms, and thermodynamic studies on the adsorption of mercury (II) ion from aqueous solution using modified palm oil fuel ash. Mater Today Proc 5:21690–21697
55. Celebi H, Gok G, Gok O (2020) Adsorption capability of brewed tea waste in waters containing toxic lead(II), cadmium (II), nickel (II), and zinc(II) heavy metal ions. Sci Rep 10:17570. https://doi.org/10.1038/s41598-020-74553-4
56. Xu X, Schierz A, Xu N, Cao X (2016) Comparison of the characteristics and mechanisms of Hg(II) sorption by biochars and activated carbon. J Colloid Interface Sci 463:55–60. https://doi.org/10.1016/j.jcis.2015.10.003
57. Lu X, Jiang J, Sun K et al (2014) Influence of the pore structure and surface chemical properties of activated carbon on the adsorption of mercury from aqueous solutions. Mar Pollut Bull 78:69–76. https://doi.org/10.1016/j.marpolbul.2013.11.007
58. Alslaibi TM, Abustan I, Ahmad MA, Abu Foul A (2015) Comparative studies on the olive stone activated carbon adsorption of Zn^{2+}, Ni^{2+}, and Cd^{2+} from synthetic wastewater. Desalin Water

Treat 54(1):166–177. https://doi.org/10.1080/19443994.2013.876672
59. Kong H, He J, Gao Y et al (2011) Cosorption of phenanthrene and mercury(II) from aqueous solution by soybean stalk-based biochar. J Agric Food Chem 59:12116–12123. https://doi.org/10.1021/jf202924a
60. Lloyd-Jones PJ, Rangel-Mendez JR, Streat M (1999) Sorption of cadmium using a natural biosorbent and activated carbon. Inst Chem Eng Symp Ser 2000 148:847–866
61. Raza MH, Sadiq A, Farooq U et al (2015) *Phragmites karka* as a biosorbent for the removal of mercury metal ions from aqueous solution: effect of modifcation. J Chem 2015:1–12. https://doi.org/10.1155/2015/293054
62. Wasewar KL, Kumar P, Chand S, Padmini BN, Teng TT (2010) Adsorption of cadmium ions from aqueous solution using granular activated carbon and activated clay. Clean-Soil, Air, Water 38(7):649–656. https://doi.org/10.1002/clen.201000004
63. Tan G, Sun W, Xu Y et al (2016) Bioresource technology sorption of mercury (II) and atrazine by biochar, modifed biochars and biochar based activated carbon in aqueous solution. Bioresour Technol 211:727–735. https://doi.org/10.1016/j.biortech.2016.03.147
64. Eom Y, Won JH, Ryu J, Lee TG (2011) Biosorption of mercury (II) ions from aqueous solution by garlic (*Allium sativum* L.) powder. J Chem Eng 28(6):1439–1443. https://doi.org/10.1007/s11814-010-0514-y
65. El-sheikh AH, Al-degs YS, Al-as RM, Sweileh JA (2011) Effect of oxidation and geometrical dimensions of carbon nanotubes on Hg(II) sorption and preconcentration from real waters. Desalination 270:214–220. https://doi.org/10.1016/j.desal.2010.11.048
66. Wang FY, Wang H, Ma JW (2010) Adsorption of cadmium (II) ions from aqueous solution by a new low-cost adsorbent—Bamboo charcoal. J Hazard Mater 177(1–3):300–306. https://doi.org/10.1016/j.jhazmat.2009.12.032